

Deep Dynamic Neural Networks for Multimodal Gesture Segmentation and Recognition

Journal:	<i>Transactions on Pattern Analysis and Machine Intelligence</i>
Manuscript ID:	TPAMISI-2015-01-0002.R1
Manuscript Type:	SI: Multimodal Human Pose Recovery and Behavior Analysis
Keywords:	Gesture Recognition, Deep Learning, 3D Convolutional Neural Networks, Deep Belief Networks

SCHOLARONE™
Manuscripts

1
2
3
4
5 August 9th, 2015
6
7
8
9 To: Editor TPAMI
10
11 TPAMISI-2015-01-0002 submission -
12 *Deep Dynamic Neural Networks for Multimodal Gesture Segmentation and Recognition.*
13
14
15 Dear Guest Editor,
16
17 This letter is in response to the review of our submitted manuscript referenced above on
18 "Deep Dynamic Neural Networks for Multimodal Gesture Segmentation and Recognition". We
19 would first like to thank the reviewers and guest editor for their time and valuable comments.
20 We have taken into careful consideration each one of these comments, and have prepared a
21 detailed response in a separate document adjoint to this letter. We have made this answer
22 as self-contained as possible to facilitate the review process. Furthermore, addressing these
23 comments led to many improvements of the manuscript. Before summarizing the main changes
24 in the paper, we would like to recall the main characteristics and contributions of the paper.
25 Within an HMM framework allowing for the simultaneous gesture recognition and segmentation,
26 we propose:
27
28
29
30
31 • A Gaussian-Bernoulli Deep Belief Network is proposed to extract high-level skeletal joint
32 features and the learned representation is used to estimate the emission probability needed
33 to infer gesture sequences;
34
35 • A learning framework is proposed to extract temporal features jointly from multiple chan-
36 nel inputs of RGB images and depth images. Because the features are learned from raw 2D
37 images stacked along the 1D temporal domain, we refer our approach as 3D Convolutional
38 Neural Network;
39
40 • Intermediate fusion and late fusion are investigated as different strategies to model emission
41 probability within the temporal modeling. Both strategies show that multiple-channel
42 fusions outperform each individual module.
43
44
45 *Major modifications:* We now would like to summarize the main changes done to the manuscript:
46
47
48 • *Intermediate fusion:* In the previous version for multimodal fusion, we used the late fusion
49 scheme $s = a * s1 + (1 - a) * s2$, where a is chosen by cross-validation. In this revision,
50 as requested and suggested by reviewer 3 and 4, we implemented an intermediate fusion
51 scheme (described in Section 4.4.2) where a new top-level perceptron layer is created
52 to combine the high-level outputs of the skeleton and RGBD networks, resulting in a
53 unified multimodal network mode as shown in Fig. 6. This intermediate fusion system uses
54 pre-trained weights, in the sense that the new multimodal neural network's parameters
55 are initialised using the parameters of the previously trained individual module, taking
56 advantage of their different intrinsic properties and making the network converge much
57 faster. The results are reported in Section 4.4.2 and Table 1.
58
59
60

- *Related Works section:* The Related Works section has been moved after the Introduction section. We also follow reviewers' comments by including discussions of suggested related works, amongst others: 1) exploiting temporal models in the context of gesture recognition, notably a discriminative hidden-state approach for the recognition of human gestures introduced by Wang *et al.* [1] ; 2) literature for RGBD data using deep learning, which includes the use of recurrent neural networks by Socher *et al.* [2] and applying convolutional neural networks on top of geocentric embedding for depth images by Gupta *et al.* [3]
- *Experimental analysis:* We have included further analysis of the temporal aspect of the model in Section 5.4, and visualisation of response maps after learnt filters in Fig 8. We also gave qualitative remarks on these filter banks. Regarding the quantitative results, we have added more analysis on failure patterns and lessons learnt from the experiments.
- *Explanation of intuition behind higher level presentation of the skeleton features:* We include Section 3.3 to explain the intuition behind higher level representation for skeleton joint features which appeared in our previous CVPR paper but was not included in the previous submission. We think this part is one of major contributions of the paper and inclusion of this section makes the journal paper more self-contained.

Minor modifications: We have addressed all reviewer's comments, most with direct modifications in the paper. We would like to highlight a few relevant points:

- *3D Convolutional Neural Networks:* We clarified accordingly to Rev4 and the readers that the 3rd dimension of the input is indeed the time axis. However, RGB and Depth data are jointly processed by the neural networks, which justifies the multiple-channel naming convention.
- *Parameters and formula interpretation* (cf Rev3): While discussing the model formulation, we have added more description and intuitive explanation about the hidden variable H_t . We also corrected and clarified the number of frames assigned to each hidden state.

We hope that these new experiments, clarifications, and paper modifications will satisfy the reviewers as well as address your own comments. We thank you again for your time and consideration of our manuscript.

Sincerely,

Di Wu, Lionel Pigou, Pieter-Jan Kindermans, Nam Le, Ling Shao, Joni Dambre, and Jean-Marc Odobez

References

- [1] S. B. Wang, A. Quattoni, L.-P. Morency, D. Demirdjian, and T. Darrell, "Hidden conditional random fields for gesture recognition," in *Computer Vision and Pattern Recognition, 2006 IEEE Computer Society Conference on*, vol. 2. IEEE, 2006, pp. 1521–1527.
- [2] R. Socher, B. Huval, B. Bath, C. D. Manning, and A. Y. Ng, "Convolutional-recursive deep learning for 3d object classification," in *Advances in Neural Information Processing Systems*, 2012.

- 1
2 [3] S. Gupta, R. Girshick, P. Arbeláez, and J. Malik, “Learning rich features from rgb-d images
3 for object detection and segmentation,” in *ECCV*. Springer, 2014.
4
5
6
7
8
9
10
11
12
13
14
15
16
17
18
19
20
21
22
23
24
25
26
27
28
29
30
31
32
33
34
35
36
37
38
39
40
41
42
43
44
45
46
47
48
49
50
51
52
53
54
55
56
57
58
59
60

Response to Reviewer 1

We thank the reviewer for his time and comments and positive appreciation of the paper. Below, we provide our answers to his comments and to the unclear points that were raised, and what we have done to clarify the paper and take comments into account. Note that in our answer, all references (Equations, Figures) refer to the new version unless stated otherwise.

Comment: *The article is easy to read and well structured. The methodology is not strictly novel but its application in the gesture domain with the multimodal fusion makes the article worth reading. Although results are arguably a little behind the maximum performance ones the overall impression of the article is favorable and I believe the community may benefit to check the ideas included in this paper.*

The article proposes a framework for dynamic data augmenting a HMM with deep learning techniques and apply this to gesture segmentation and recognition. Gestures segmentation and recognition is a difficult problem. The article tackles this difficulty by means of pure data driven approaches similar to the ones used for speech recognition. The particularities of the computer vision domain are handled accordingly.

Response: Thank you for your review and positive outlook of the paper. We are also aware that our results are arguably a little behind the maximum performance, and this may be due to the network initialisation and multimodal neural network learning.

Note that the revised version has undergone an important rewriting which hopefully should further improve the clarity of the method description, as well as the DBN and 3DCNN motivation (Section III-C). It also includes extra experimental analysis and an extra intermediate fusion implementation and evaluation to further extend the broadness of the paper.

Response to Reviewer 2

We thank the reviewer for his time and comments. Note that the article has been reworked significantly to better introduce and enhance the modeling elements and their motivation (see Section III-C). In addition, further experiments with an intermediate fusion scheme learning a joint multimodal representation have been conducted. Below, we provide our specific answers to his comments and to the unclear points that were raised, and what we have done to clarify the paper and take comments into account. Note that in our answer, all references (Equations, Figures) refer to the new version unless stated otherwise.

Comment: *In general, the manuscript is well written and is easy to follow. In the given case, it would be preferable to have the "Related work" section right after the introduction, as otherwise paper's contributions are not completely clear. Furthermore, there is certainly a vast literature on exploiting HMMs in the context of gesture recognition (as well as other temporal models, such as recurrent neural networks), which should be briefly summarized, the differences with the proposed solution should be highlighted.*

Response: Thank you for your comments and the recognition of easy readability of the paper. We agree that in this journal version of the paper, some self-contained information had been omitted from the conference paper, and that there were unclear points. We have moved the related work section after the introduction section. Moreover, we have included the discussions of literature that utilise temporal models, e.g.“Wang *et al.* [37] introduced a more elaborated discriminative hidden-state approach for the recognition of human gestures. However, relying on only one layer of hidden states, their model alone might not be powerful enough to learn a higher level representation of the data and take advantage of very large corpus. In this paper, we adopt a different approach by focusing on deep feature learning within a temporal model.” We also include more literatures discussing the benefits of deep learning using RGB-D data for object detection or classification tasks such as:“Socher *et al.* [39] proposed a single convolutional neural net layer for each modality as inputs to multiple, fixed-tree RNNs in order to compose higher order features for 3D object classification. The single convolutional neural net layer provides useful translational invariance of low level features such as edges and allows parts of an object to be deformable to some extent.” Regarding your concern about the novelty of each individual technique, we agree that the hybrid combination of HMM and ANN can be traced back to earlier works in continuous speech recognition [33] [32]. However, it is important to point out that the problem we addressed includes not only learning emission probability but also learning features from raw multi-stream of inputs which do not share the same characteristics. To our best knowledge, this problem has not been explored before in the context of gesture recognition. This can be further argued by comparing with other state-of-the-art works which rely on hand-crafted features to some degree [57] [43].

We have significantly reworked the paper and improved its structure to both improve clarity and account for the reviewer’s comment.

- Section III now describe the method overview, both in terms of HMM modeling with more intuition about the temporal modeling(Section III-A and III-B), and in terms of Neural network modeling (Section III-C), including with new figures;
- more motivation and intuition behind the use of learned higher level representation and the advantages offered by DBN models for emission probability modeling over the use of GMMs, including the crucial importance of the Gaussian-Bernouilli Restricted Boltzman Machines for pretraining and initializing the deep belief network.
- the experimental part includes a proper description of the dataset, experimental protocol (including performance measures), and more result analysis.
- finally, an intermediate fusion scheme that learns a shared representation has also been implemented and evaluated. Its description is provided in Section V-C.

We hope and believe that this revision is now much more self-contained and will better suit the quality standard of a journal paper.

Comment: Authors claim to learn a model in the joint multi-modal space is a slight overstatement, as neural networks processing different modalities are trained completely independently with following averaging of produced scores.

Response: Thank you for your comments. In this revision, we implement the intermediate fusion scheme in Section IV-D2 that we adopt another layer of perceptron for cross modality learning taking the input from each individual net's penultimate layer. The parameters of two neural networks (for skeleton and depth) are loaded from the previously trained individual module. The results for the intermediate fusion system are reported in Tab. I. The fusion network is initialised by the pre-trained model and stacked with one hidden layer with 2024 hidden units. We fine-tune the network and stop the training when the validation error rate stops decreasing (~ 15 epochs). However, we can see from Tab. I that the intermediate fusion system does not outperform the late fusion system. The result is counter-intuitive because we expect that the intermediate fusion multimodal feature learning would extract semantically meaningful shared representations, outperforming individual modalities, and the intermediate fusion schemes efficacy against the traditional method of late fusion [65]. One possible explanation could be that one individual module has dominant effect on the learning process so as to skew the network towards learning that specific module. The mean activations of the neurons for each module in Fig. 6 indicate the aforementioned conjecture: the large difference between the mean activations of the skeleton module neurons which are predominantly larger than those of the RGB-D ConvNet's (0.57 vs. 0.056) can be an indicator of such a bias during the multimodal fine-tuning phase and support this conjecture, even if these mean activations are not directly comparable due to the neuron heterogeneity (the skeleton DBN has logistic units whereas the 3DCNN ConvNet has relu units). Note that such heterogeneity was not present when fusing modalities in [22], where better registration and less spatial registration variability in lip images allowed to also resort to the same stacked RBMs for the visual modality (rather than 3DCNN) and the audio one. More investigation on how to handle heterogeneous networks should be conducted.

Comment: State of the art in the experimental section should be mentioned more consistently. For fair comparison, first three lines in Table 3 should be: [39] Deep learning (step 4): skeleton 0.7891, video 0.7990, fusion 0.8449 [39] Deep learning (multiscale): skeleton 0.8080, video 0.8096, fusion 0.8488 [40] 3 sets of skeletal features and HoG: skeleton 0.791, fusion 0.8220 Therefore, it shows that both learning-based and feature extraction-based approaches outperform the proposed method on each modality, as well as on a combination of them. Furthermore, it would be interesting to see how the HMM contributes in the performance in comparison with simple voting based on frame-based predictions.

Response: Thank you for your detailed comments. We have amended the results table accordingly. The less than maximum performance could be due to the less than ideal settings and initialisations of the neural network. Nonetheless, we would like to argue that one major contribution of the paper is using the learning method for feature extraction and the utilisation of HMM for simultaneous gesture segmentation and recognition. We also present some brief analysis of why the fusion network didn't achieve expected performance gain and hope the experimental analysis could cast some light on the future research directions of the related problems.

Comment: Visualization of the filter banks (section 3.3.4) in its current state is unnecessary as it does not provide any interesting insights on the interpretation of the learned features. Instead, the poorly formed filters rather indicate undertraining, or lack of training data given the model complexity, or suboptimality of training procedure.

1
2
3 **Response:** In the revision, we include the response maps after filtering for both body and hand parts as in Fig. 5. Because our
4 filter size is 5×5 (smaller filter sizes tend to generalize better, [66] used 3×3 convolution filters), their interpretation is indeed
5 harder to visualise, although one can notice that depth filters capture smooth depth transitions, and the combined image and
6 depth filter (see architecture description in Section IV-C2 and Fig. 5) can represent two types of information: segmentation, and
7 edge. We have modified the text to provide better insight as follows:
8

9
10 *“The convolutional filter weights of the first layer are depicted in Fig. 5. The unique characteristics from the kernels are clearly
11 visible: as hand input images (RGB and depth) have larger homogenous areas than the body inputs, the resulting filters are
12 smoother than their body counterpart. In addition, while being smoother overall than the grayscale filters, depth filters exhibit
13 stronger edges, as also reported in [39]. Finally, by looking at the joint depth-image response maps, we can notice that some
14 filters better capture segmentation like information, while other are more edge oriented.”*
15

Response to Reviewer 3

We thank the reviewer for his time and insightful comments. Below, we provide our specific answers to his comments and to the unclear points that were raised, and what we have done to clarify the paper and take comments into account. Note that in our answer, all references (Equations, Figures) refer to the new version unless stated otherwise.

Comment: *The paper proposes the fusion of the output from a Gaussian-Bernoulli Deep Belief network operating on skeletal features and the output of a Convolutional Neural Network operating on RGBD data to perform gesture segmentation and recognition. The paper advances the field of gesture recognition by using both data sources and deep learning architectures within a Hidden Markov Model chain. The results are improved compared to using either architecture independently.*

In general, I would be more excited if shared representations were learned from the skeleton and the RGB data, as done in multimodal deep learning. This is left for future work. The paper might not have enough new material to warrant a PAMI publication wrt to the previous conference versions. I also find that it is not that well written for a journal paper (see below). On the positive side, the CNN and DBN are technically sound and the results from their fusion are interesting.

One would expect that the journal version of the paper would be more self-contained and easier to follow than the conference versions, but here I observe the opposite trend. For example, the older conference version [21] explains the intuition behind the higher level representation of the skeleton features, but the journal version does not. The conference paper explains how the coordinate frames are built for the features, while this paper skips this part. The conference paper explains the datasets and visualizes the Viterbi paths better.

Response: Thank you for your careful and positive review. We agree that in this journal version of the paper, some self-contained information had been omitted from the conference paper, and that there were unclear points. We have significantly reworked the paper and improved its structure to both improve clarity and account for the reviewer's comment:

- a related works section has been added;
- Section III now describe the method overview, both in terms of HMM modeling (Section III-A and III-B), and in terms of Neural network modeling (Section III-C), including with new figures;
- more intuition about the temporal modeling (Section III-A);
- more motivation and intuition behind the use of learned higher level representation and the advantages offered by DBN models for emission probability modeling over the use of GMMs, including the crucial importance of the Gaussian-Bernoulli Restricted Boltzman Machines for pretraining and initializing the deep belief network.
- the experimental part includes a proper description of the dataset, experimental protocol (including performance measures), and more result analysis.
- finally, an intermediate fusion scheme that learns a shared representation has also been implemented and evaluated. Its description is provided in Section V-C. However, to the contrary of what we had expected, it did not perform better than the late fusion scheme.

We hope and believe that this revision is now much more self-contained and will better suit the quality standard of a journal paper.

Comment: *Section 2 does not help much the reader understand the formulation. For example: "At each time step, we have one observed random variable X_t : explain what these variables represent early (raw skeletan input / RGB-D) we have an unobserved variable H_t : describe at a high level the information that the unobserved variables capture, mention examples*

Response: We have considerably reworked Section III to provide an overview of the method along with intuition and motivations. Please check the new version. More specific parts of this section addressing your more specific comments are provided below.

1
2
3 Regarding the variables:
4
5

6 “A continuous-observation HMM is adopted for modelling higher level temporal relationships. At each time step t , we have
7 one observed random variable X_t composed of the skeleton input X_t^s and RGB-D input images X_t^r as shown in the graphical
8 representation in Fig. 1. The hidden state variable H_t takes on values in a finite set \mathcal{H} composed of $N_{\mathcal{H}}$ states related to the
9 different gestures. The intuition motivating the HMM model is that a gesture is composed of a sequence of poses where the
10 relative duration of each pose may vary. This variance is captured by allowing flexible forward transitions within a Markov
11 chain. In practice, H_t can be interpreted as being in a particular phase of a gesture \mathbf{a} . ”
12

13 Or related to more concrete example (Section III-B abut Markov state diagram):
14

15 “For each given gesture $a \in \mathcal{A}$, a set of states \mathcal{H}_a is introduced to defined a Markov model of that gesture. For example, for
16 action sequence “tennis serving”, the action sequence can implicitly be dissected into $h_{a_1}, h_{a_2}, h_{a_3}$ as: 1) raising one arm 2)
17 raising the racket 3) hitting the ball. ”
18

19
20
21 **Comment:** The related work section is out of place after the technical sections and before the experiments.
22

23 **Response:** We have now written a proper related work section after the introduction section.
24

25 **Comment:** There is no point writing a loop for $m=1:2$ in Algorithm 1 and 2.
26

27 **Response:** The Algorithm description has been removed from the paper. We have privileged a more structured and more textual
28 description of the method, and thus needed to remove the Algorithms for space reason. Nevertheless, we believe that given
29 the method overview in Section III, and the more detailed elements in Section IV, the method steps should be fairly easily
30 understandable.
31

32 **Comment:** “the number of states ... is chosen as 5”: any intuition here?
33

34 **Response:** Thank you for the comment and this is a very good observation. The main intuition behind this number was that
35 a gesture is often composed of 5 phases: 1) an onset; 2) arm motions to reach 3) a more static pose (often characterized by
36 a distinct hand posture); and 4) motion back to 5) stop in the rest pose. However, we agree that this number might not be
37 optimal, and that different gestures could have different number of states. Also, from a more heuristic point of view, note that
38 we had performed experiments with 10 states per class, and that it performed similarly.
39

40 To account for the reviewer’s comment we have updated the text as follows:
41

42 “Note that intuitively, 5 states represents a good granularity as most gestures in the Clalearn are composed of 5 phases: an
43 onset, followed by arm motions to reach a more static pose (often characterized by a distinct hand posture), and the motion
44 back to the rest place. In the future, optimal selection of this number⁶ and of different number of states per gesture could be
45 investigated. ”
46

47 **Comment:** “10 frames are assigned to hidden state ...”: why 10?
48

49 **Response:** Thank you for the careful observation. This is actually a written error. The corrected text reads now:
50

51
52
53
54
55
56
57
58
59
60 ⁶Experiments with 10 states led to similar performance.

“To do so, a force alignment is used which means that if the i^{th} sequence is a gesture \mathbf{a} , then the first $\lfloor \frac{T_i}{5} \rfloor$ frames are assigned to state $h_{\mathbf{a}}^1$ (the first state of gesture \mathbf{a}), the following $\lfloor \frac{T_i}{5} \rfloor$ frames are assigned to $h_{\mathbf{a}}^2$, and so forth.”

Comment: it is hard to interpret the learned features on Figure 8. There is no intuition what the depth filters capture.

Response: Because our filter size is 5×5 (smaller filter sizes tend to generalize better, [66] used 3×3 convolution filters), their interpretation is indeed harder to visualise, although one can notice that depth filters capture smooth depth transitions, and the combined image and depth filter (see architecture description in Section IV-C2 and Fig. 5) can represent two types of information: segmentation, and edge. We have modified the text to provide better insight as follows:

“The convolutional filter weights of the first layer are depicted in Fig. 5. The unique characteristics from the kernels are clearly visible: as hand input images (RGB and depth) have larger homogenous areas than the body inputs, the resulting filters are smoother than their body counterpart. In addition, while being smoother overall than the grayscale filters, depth filters exhibit stronger edges, as also reported in [39]. Finally, by looking at the joint depth-image response maps, we can notice that some filters better capture segmentation like information, while other are more edge oriented.”

Comment: Citations that could be added in the context of deep learning from RGBD data: “Convolutional-Recursive Deep Learning for 3D Object Classification”, Socher et al., NIPS 2012, and “Learning Rich Features from RGB-D Images for Object Detection and Segmentation”, Gupta et al., ECCV 2014.

Response: Thank you for the suggested citations. We find those work interesting, e.g. for Gupta et al. [40], as it shows that CNN do not necessarily need to be trained from the raw images, and some handcrafted features may better help the network to learn more meaningful, higher level representations. We have added these references in the paper in the following way:

“However, the advent of Kinect-like sensors has put more emphasis on RGB-D data for gesture recognition, but not only. For instance, the benefits of deep Learning using RGB-D data have been explored for object detection or classification tasks. Socher et al. [39] proposed a single convolutional neural net layer for each modality as inputs to multiple, fixed-tree RNNs in order to compose higher order features for 3D object classification. The single convolutional neural net layer provides useful translational invariance of low level features such as edges and allows parts of an object to be deformable to some extent. To address object detection, Gupta et al. [40] proposed a geocentric embedding for depth images that encodes height above ground and angle with gravity for each pixel in addition to the horizontal disparity.”

Comment: Another related work is the “Multimodal Deep Learning” by Ngiam et al., ICML 11. I would also like to see some discussion wrt “Hidden Conditional Random Fields for Gesture Recognition”, Wang et al., CVPR 2006

Response: Thank you for suggesting very relevant works. We came across both papers. “Multimodal Deep Learning” essentially is the prototype for an intermediate fusion model. Regarding Wang et al. [37]), the similarity with our proposed method is that both methods use a/several hidden layer for learning higher level representations. However, authors in Wang et al. [37]) observed that one hidden layer is limited for learning a larger class corpus. In our case, we believe that higher level representation learning with more layers, which is an essential part of our paper, is very important for gesture classification. Recent advancement in multi-layer feature learning and pre-training for DBN renders our proposed method more meaningful. We have included the references as follows:

For Ngiam et al, as it does not relate to gesture recognition, we have cited this method in the introduction.

1
2
3 “ Multimodal deep learning technique were also investigated [22] to learn cross-modality representation, for instance in the
4 context of audio-visual speech recognition. ”
5

6 However, as their method is very similar to the intermediate fusion scheme we have now implemented, we have added the
7 following in Section IV-D2:
8

9 “ Note that this is very similar to the approach proposed in [22] for audio-visual speech recognition. An important difference is
10 that in [22], the same stacked RBMs/DBN architecture was used to represent both modalities before fusion, whereas in our case,
11 a stacked RBMs/DBN and a 3DCNN are used. Also, [22] proposed the use of a multimodal autoencoder to handle predictions
12 when potentially only one modality might be present, a point that we do not address. ”
13

14 For Wang et al:
15

16 “ Wang et al. [37] introduced a more elaborated discriminative hidden-state approach for the recognition of human gestures.
17 However, relying on only one layer of hidden states, their model alone might not be powerful enough to learn a higher level
18 representation of the data and take advantage of very large corpus. In this paper, we adopt a different approach by focusing on
19 deep feature learning within a temporal model. ”
20
21
22
23
24
25
26
27
28
29
30
31
32
33
34
35
36
37
38
39
40
41
42
43
44
45
46
47
48
49
50
51
52
53
54
55
56
57
58
59
60

Response to Reviewer 4

We thank the reviewer for his time and insightful comments. Below, we provide our specific answers to his comments and to the unclear points that were raised, and what we have done to clarify the paper and take comments into account. Note that in our answer, all references (Equations, Figures) refer to the new version unless stated otherwise.

Comment: *The paper purports 3 contributions. (1) the authors use deep learning to estimate emission probabilities for a HMM predicting gesture. (2) They use a 3d convolutional network. While the introduction makes it sound like this is for multiple-channels (e.g. RGB + Depth), sec. 3.3.2 makes it clear the 3rd dimension is time as the model processes 4 frame sub-sequences. I think, Fig. 6 could be clearer. (3) Emission probability models are trained for both the skeletal data and depth data. They are then averaged (weighted) and used in an HMM.*

Overall, I am convinced this paper solves the problem of gesture recognition with a novel combination of techniques. However, I am not convinced (1) any of the technical techniques themselves are particularly novel nor (2) that the chosen combination is the right one. Finally, (3) the results aren't particularly impressive (only matching state-of-the-art). Moreover, I have technical/philosophical objections which I'll elaborate on in the comments.

Learning to model HMM emission and transition parameters is an old idea (going back decades, to at least the well known Baum-Welch algorithm) and 3D convolutional networks for video were explored by [11].

Using RGB-D with deep learning is a common idea, explored by many concurrent works e.g. [A,B,C]. [A] Dosovitskiy, A., Springenberg, J. T., Riedmiller, M., Brox, T. (2014). Discriminative Unsupervised Feature Learning with Convolutional Neural Networks. Arxiv Preprint arXiv: 1-13. [B] Gupta, S., Girshick, R., Arbelez, P., Malik, J. (2014). Learning Rich Features from RGB-D Images for Object Detection and Segmentation. arXiv Preprint arXiv:1407.5736, 116. doi:10.1007/978-3-319-10584-0 23 [C] Socher, R., Huval, B., Bhat, B., Manning, C. D., Ng, A. Y. (2012). Convolutional-Recursive Deep Learning for 3D Object Classification. Advances in Neural Information Processing Systems 25, (i), 665-673.

Response: Thanks for the comments. Note that we have significantly reworked the paper and improved its structure to both improve clarity and make the paper more self-contained, while taking into account reviewers' comments. Regarding your specific issues above, we can state the following and have made the following changes:

- Regarding your concern about the novelty of each individual technique, we agree that the hybrid combination of HMM and ANN can be traced back to earlier works in continuous speech recognition [33] [32]. However, it is important to point out that the problem we addressed includes not only learning emission probability but also learning features from raw multi-stream of inputs which do not share the same characteristics. To our best knowledge, this problem has not been explored before in the context of gesture recognition. This can be further argued by comparing with other state-of-the-art works which rely on hand-crafted features to some degree [57] [43].

In response to your question if we have chosen the right combination, it is true that there are several techniques appropriate for each model, some of which are presented in Related Works. Nonetheless, given the limited scope of the paper we focus on the combination which has the most potential. For each module, we can justify our choice of techniques as following: First, at the feature learning stage, we have to deal with 3 input streams: skeleton input, RGB images, and depth images. RGB images and depth images share correlated spatial information. We believe it is the right choice to learn features jointly by combining these two streams as a single 2-channel input. By expanding the CNN into temporal domain, the learnt features extracted by 3DCNN not only describe high level visual but also dynamic information about movements. On another hand, skeleton input appears to be sparser but contains more robust information. DBN architecture initialised with Gaussian-Bernoulli RBM can exploit high level correlation among the set of upper body joints and the learnt features

also can be compatible with features learnt from 3DCNN. Secondly, at the temporal modeling stage, HMM is a clearly a very good candidate given its pros in simultaneous segmentation and inference. Therefore, we followed the previous works in speech recognition and embedded our dynamic deep neural networks in HMM. With the points noted out, we believe our paper has sufficient novelty and contributions, and very much deserves publication in a TPAMI devoted to the gesture recognition task.

- Regarding the 3DCNN. It was not our intention to confuse the reader. We have made the text more explicit in the introduction:

“A 3D Convolutional Neural Network is proposed to extract features from 2D multiple channel inputs like depth and RGB images stacked along the 1D temporal domain;”

and similarly, when presenting the 3DCNN in section Section IV.C.2

“The 3D convolution itself is achieved by convolving a 3D kernel to the cuboid formed by stacking multiple contiguous frames together.”

We have also updated the 3DCNN figure (now figure 4 in the paper), specifying the input, intermediate layers and their corresponding modalities more explicitly, which we hope is not ambiguous.

- multimodal fusion: we have now implemented and evaluated a more unified neural network to this end. See the answer to your next comment.
- Related work. Thank you for suggesting very relevant works using RGB-D with deep learning. We have included them in the related litterature as follows:

“However, the advent of Kinect-like sensors has put more emphasis on RGB-D data for gesture recognition, but not only. For instance, the benefits of deep learning using RGB-D data have been explored for object detection or classification tasks. Dosovistskiy et al. [38] presented a generic feature learning for training a convolutional network using only unlabeled data. In contrast to supervised network training, the resulting feature representation is not class specific and are advantageous on geometric matching problems, outperforming the SIFT descriptor. Socher et al. [39] proposed a single convolutional neural net layer for each modality as inputs to multiple, fixed-tree RNNs in order to compose higher order features for 3D object classification. The single convolutional neural net layer provides useful translational invariance of low level features such as edges and allows parts of an object to be deformable to some extent. To address object detection, Gupta et al. [40] proposed a geocentric embedding for depth images that encodes height above ground and angle with gravity for each pixel in addition to the horizontal disparity. This augmented representation allows CNN to learn stronger features than when using disparity (or depth) alone.”

Comment: Late fusion: my greatest technical concern is that two deep models are trained and then combined with a weighted average: $s = a * s1 + (1-a)*s2$ where a is chosen by cross-validation. Instead, the authors could combine the two models by creating a new top-level perceptron layer which takes the two models as input. Then this whole structure could be trained jointly with back-propagation. I'd expect results to be (1)at least as good and (2) more philosophically unified.

Response: We agree with your insightful observation, and actually believe that this should improve the system. We thus implemented and evaluated such an intermediate fusion scheme in this revision. However, this approach did not improve the results over the late fusion scheme, providing similar results.

To account for this new model, the text was updated as follows in the model description and the result analysis. In Section IV-D2, describing the Intermediate fusion:

“ As an alternative to the late fusion scheme, we can take advantage of the high-level representation implicitly learned by each module (and represented by the V^s and V^r nodes of the penultimate layer of the respective networks, before the softmax) to fuse the modality in an intermediate fashion by concatenating these two layers in one layer of 2024 hidden unites and learning a cross-modality emission probability predictive network. Note that this is very similar in spirit to the approach proposed in [22] for audio-visual speech recognition. An important difference is that in [22], the same stacked RBMs/DBN architecture was used to represent both modalities before fusion, whereas in our case, a stacked RBMs/DBN and a 3DCNN are used. Also, [22] proposed the use of a multimodal autoencoder to handle predictions when potentially only one modality might be present, a point that we do not address.

The resulting architecture is trained by first initializing the weights of the deeper layers from the previously trained module, and then jointly fine tuning the whole network (including learning the last layer parameters) and stop the training when the validation error rate stops decreasing (~ 15 epochs). We argue that using the “pre-trained” parameters is important due to the heterogeneity of the inputs of the system, and that the joint training should adjust parameters to handle this heterogeneity and produce the final estimates. ”

A specific section in the analysis is devoted to the result analysis, which reads:

“ **Late vs. Intermediate fusion.** The results in Tab. I and II show that the intermediate fusion system improved individual modalities, but without outperforming the late fusion system. The result is counter-intuitive, as we would have expected the cross-modality learning in the intermediate fusion scheme to result in better emission probability predictions, as compared to the simple score fusion in the late system. One possible explanation is that the independance assumption of the late scheme better preserves both the complementarity and redundancy of the different modalities, properties which are important for fusion. Another related explanation is that in the intermediate fusion learning process, one modality may dominate and skew the network towards learning that specific module and lowering the importance of the other one. The large difference between the mean activations of the skeleton module neurons which are predominantly larger than those of the RGB-D ConvNet’s (0.57 vs. 0.056) can be an indicator of such a bias during the multimodal fine-tuning phase and support this conjecture, even if these mean activations are not directly comparable due to the neuron heterogeneity (the skeleton DBN has logistic units whereas the 3DCNN ConvNet has relu units). Note that such heterogeneity was not present when fusing modalities in [22], where better registration and less spatial registration variability in lip images allowed to also resort to the same stacked RBMs for the visual modality (rather than 3DCNN) and the audio one. More investigation on how to handle heterogeneous networks should be conducted. ”

Comment: The analysis is a bit brief. More experiments and ablative analysis could be added. Specifically, can we interpret the failure patterns of the proposed model(s) and prior work? It would be interesting to see statements like [40] fails more often on gestures of X kind because HOG erases Y useful information or [39] does worse for Z because it handles time at an earlier stage of the pipeline. Then, also giving some qualitative examples of these failures.

Response: We agree that there is a lack of experiments analysis, especially the failure patterns and lessons learnt from the experiments. We have included more analysis in the Experiment and Analysis, see the whole section V.C. Below we provide the text related to major changes:

(1) discussion of confusion matrices:

“ The confusion matrices (in log-form) in Fig. 9 better illustrate the complementarity of the behaviors of the two modalities.

The higher underdetection of RGB-D is clearly visible (whiter matrix, except last 'undetected' column). We can also notice that some gestures are more easily recognized than others, or catch the difficult instances of other gestures. This is the case of the "Basta" gesture, whose arms motion resembles the start and end of the arm motion of many other gesture (see Fig. 7). Whatever the modality, its model thus tends to recognize few instance of all other gesture classes, whenever their likelihood are low when being evaluated using the HMM states associated with their true label due to too much variability. Similarly, the hand movement and pose of the "Buenissimo" gesture is present in several other gesture classes, whose instances are then often confused with "Buenissimo" when relying on the skeleton information alone. However, as these gestures differ primarily in their hand pose, such confusion is much more reduced using the RGB-D domain, or when fusing the skeleton and RGB-D modules. The complementary properties of the two modalities is also illustrated from the Viterbi path decoding plot in Fig. 8. In general, the benefit of this complementarity between arm pose/gesture and hand pose can be observed from the whiter confusion matrix than in the skeleton case (less confusion due to hand pose information from RGB-D) and much less under-detection than in the RGB-D case (better upper-body pose discrimination thanks to skeleton input).

However, the modalities by themselves have more difficulties to correct the recognition errors which are due to variations coming from the performer, like differentiating people that gesticulate more (see Fig. 11). ”

(2) discussion of late and intermediate feature fusion (see answer to your previous comment).

(3) analysis of the temporal modelling benefits:

“**HMM benefit.** As the emission probabilities are learned in a discriminative manner, one could wonder whether the HMM brings benefit beyond smoothing. To investigate this issue, we removed the temporal structure as follows: for a given gesture \mathbf{a} , we computed its score at time t , $\text{Score}(\mathbf{a}, t)$, by summing the emission probabilities $p(X_t | H_t = h)$ for all nodes associated to that gesture, i.e. $h \in \mathcal{H}_\mathbf{a}$. This score is then smoothed in the temporal domain (using a window of 5 frames) to obtain $\widehat{\text{Score}}(\mathbf{a}, t)$. Finally, following [57], the gesture recognition proceeds in two steps: first finding gesture segments by thresholding the score of the ergodic state; then, for each resulting gesture segment, the recognized gesture is defined as the one whose average score within the segment is the highest. Fig. 10 illustrates this process along with the DDNN and ground-truth. In general, we could observe that better decisions on the presence of gestures and on the boundaries where a gesture starts and ends are achieved with the proposed DDNN thanks to the use of the state-diagram defined in Fig. 2, as compared to the above method, where deciding on a gesture detection threshold is rather unstable and quite sequence dependent. Indeed, the overall performance of the above scheme without the HMM temporal sequencing is reduced to $J\bar{I} = 0.66$, while the Recognized, Confused and Missed corresponding to Table II for the test set are 76.6 , 5.3 and 18.1. However, note that the above method relying on only the gesture probability learned using neural networks on 5 frame inputs still outperforms the Jaccard index of 0.413 obtained by [58] when using a 5 frames template matching system where all the features are handcrafted. ”

(4) better understanding of the challenges of the dataset caused by different performers' body movement, as illustrated in Fig. 11:

“ Most performers tend to keep their upper-body static while performing the gesture, leading to good recognition performance (Jaccard index of person on the top is 0.95 for the late fusion system). Some persons are more involved and move more vehemently (person at the bottom, Jaccard index of 0.61), which can affect the recognition algorithm itself (bottom left samples) or even the skeleton tracking (bottom right; note that normally cropped images are centered vertically on the head position).

Examples of overall upper body movements influence on the system performance. Left (score: 0.94) performer almost kept a static upper body whilst performing Italian sign language. Right (score: 0.34) performer moved vehemently when performing

1
2
3 the gestures.11 ”
4
5
6
7
8
9
10
11
12
13

Comment: These extra experiments (considering joint training of a combined emission probability model) and qualitative interpretation could significantly affect the paper. Overall, the research is solid but needs significantly more work before publication. RCNN: Last, it is entirely possible to train a recurrent neural network to perform Viterbi decoding. This may be difficult (requiring more training data) but would make the entire paper fit into a the deep learning framework. I cannot hold this against the authors, but some discussion might help.

Response: We have developed such a joint training and included more qualitative interpretation of the results. We agree that a recurrent neural network could potentially replace the Viterbi decoding part to make the system as a more unified end-to-end system. This, however, may be left to the future work, and have included the following in the conclusion:

“ In addition, while the proposed HMM provided a good basis for the temporal modeling of gestures, other more discriminant temporal approaches such as Conditional Random Field or further and better variants [37] could be directly exploited at their advantage in conjunction with our deep neural network learning approach. Ultimately, in a logical way, these two research directions converge into the investigation of a single and unified deep learning framework fusing heterogeneous modalities by using recent Recurrent Neural Networks such as Long Short Term Memory [64] for modelling the temporal component of the problem. ”

Comment: They use a 3d convolutional network. While the introduction makes it sound like this is for multiple-channels (e.g. RGB + Depth), sec. 3.3.2 makes it clear the 3rd dimension is time as the model processes 4 frame sub-sequences. I think, Fig. 6 could be clearer.

Response: See earlier our answer to this issue.

Deep Dynamic Neural Networks for Multimodal Gesture Segmentation and Recognition

Di Wu, Lionel Pigou, Pieter-Jan Kindermans, Nam Le, Ling Shao, Joni Dambre,
and Jean-Marc Odobez

Abstract

This paper describes a novel method called deep dynamic neural networks (*DDNN*) for multimodal gesture recognition. More precisely, a semi-supervised hierarchical dynamic framework based on a Hidden Markov Model (HMM) is proposed for simultaneous gesture segmentation and recognition where skeleton joint information, depth and RGB images are the multimodal input observations. Unlike most traditional approaches which rely on the construction of complex handcrafted features as HMM input features, our approach learns high-level spatio-temporal representations using deep neural networks suited to the input modality: a Gaussian-Bernoulli deep belief networks (*DBN*) to handle skeletal dynamics, and a 3D convolutional neural networks (*3DCNN*) to manage and fuse batches of depth and RGB images. This achieved through the modeling and learning of the emission probabilities of the HMM required to infer the gesture sequence. This purely data driven approach achieves a score of **0.81** in the ChaLearn LAP gesture spotting challenge. The performance is on par with a variety of the state-of-the-art hand-tuned feature based approaches and other learning based methods. Thus opening the door for using deep learning techniques to further explore multimodal time series.

Index Terms

Deep learning, convolutional neural networks, deep belief networks, hidden Markov models, gesture recognition.

I. INTRODUCTION

In recent years, human action recognition has drawn increasing attention of researchers, primarily due to its potential in areas such as video surveillance, robotics, human-computer interaction, user interface design, and multimedia video retrieval.

Previous works on video-based motion recognition [1]–[3] mainly focused on adapting handcrafted features. These methods usually have two stages: an optional feature detection stage followed by a feature description stage. Well-known feature detection methods (“interest point detectors”) are Harris3D [4], Cuboids [5] and Hessian3D [6]. For descriptors, popular methods are Cuboids [7], HOG/HOF [4], HOG3D [8] and Extended SURF [6]. In recent work of Wang *et al.* [9], dense trajectories with improved motion based descriptors epitomised the pinnacle of handcrafted features and achieved state-of-the-art results on a variety of “in the wild” datasets. Based on the current trends, challenges and interests within the action recognition community, it is to be expected that many successes will follow. However, the very high-dimensional and dense trajectory features usually require the use of advanced dimensionality reduction methods to make them computationally feasible.

Furthermore, as discussed in the evaluation paper of Wang *et al.* [10], no universally best hand-engineered feature exists and the best performing feature descriptor is often dataset dependent. This clearly indicates that the ability to learn dataset specific feature extractors can be highly beneficial. For this reason, even though handcrafted features have dominated image recognition in previous years, there has been a growing interest in learning low-level and mid-level features, either in supervised, unsupervised, or semi-supervised settings [11]–[13].

Since the recent resurgence of neural networks invoked by Hinton and others [14], deep neural architectures serve as an effective solution for extracting high-level features from data. Deep artificial neural networks have won numerous contests in pattern recognition and representation learning. Schmidhuber [15] compiled a historical survey compactly summarising relevant works with more than 850 entries of credited works. From this overview we see that these models have been successfully applied to a plethora of different domains: the GPU-based cuda-convnet [16] classifies 1.2 million high-resolution images into 1000 different classes; multi-column deep neural networks [17] achieve near-human performance on the handwritten digits and traffic signs recognition benchmarks; 3D convolutional neural networks [18] [19] recognise human actions in surveillance videos; deep belief networks combined with hidden Markov models [20] [21] for acoustic and skeletal joints modelling outperform the decade-dominating paradigm of Gaussian mixture models in conjunction with hidden Markov models. Multimodal deep learning technique were also investigated [22] to learn cross-modality representation, for instance in the context of audio-visual speech recognition. And recently, Baidu research proposed a DeepSpeech system [23] that combines a well-optimised recurrent neural network (RNN) training system, achieving the best error rate on noisy speech dataset. In these fields, deep architectures have shown great capacity to discover and extract higher level relevant features.

However, direct and unconstrained learning of complex problems remains difficult, since (i) the amount

of required training data increases steeply with the complexity of the prediction model and (ii) training highly complex models with very general learning algorithms is extremely difficult. It is therefore a common practice to restrain the complexity of the model. This is generally done by operating on small patches to reduce the input dimension and diversity [13], or by training the model in an unsupervised manner [12], or by forcing the model parameters to be identical for different input locations (as in convolutional neural networks [16]–[18]).

On the sensor side, due to the immense popularity of Microsoft Kinect [24] [25], there has been a recent interest in developing methods for human gesture and action recognition from 3D skeletal data and depth images. A number of new datasets [26]–[29] have provided researchers with the opportunity to design novel representations and algorithms, and test them on a much larger number of sequences. While gesture recognition based on 3D joint positions may seem trivial, it is actually not the case due to several factors. A first one is the high dimensionality and the large amount of variability of the pose space itself. A second aspect that further complicates the recognition is the segmentation of the different gestures. While in practice segmentation is as important as the recognition, it is an often neglected aspect of the current action recognition research which often assume the availability of segmented inputs [4] [30] [31].

In this paper we aim to address these issues by proposing a data driven system, focusing on analysis of acyclic video sequence labelling problems, *i.e.* video sequences that are non-repetitive as opposed to longer repetitive activities, *e.g.* jogging, walking and running. By integrating deep neural networks within an HMM temporal framework, our work allows the online joint recognition and segmentation of gestures. This framework is inspired by discriminant HMM, which embedded multi-layer perceptron inside HMM, in continuous speech recognition [32] [33]. This paper is an extension of the works of [21], [34] and [35]. The key contributions can be summarised as follows:

- A Gaussian-Bernoulli Deep Belief Network is proposed to extract high-level skeletal joint features and the learned representation is used to estimate the emission probability needed to infer gesture sequences;
- A 3D Convolutional Neural Network is proposed to extract features from 2D multiple channel inputs like depth and RGB images stacked along the 1D temporal domain;
- Intermediate and late fusion strategies are investigated within the temporal modelling. The result of both mechanisms show that multiple-channel fusions outperform individual modules.

The remainder of this paper is organised as follows. Section II reviews related works for gesture recognition with various temporal models and recent deep learning work on RGB-D data. Section III introduces the formulation of our Deep Dynamic Neural Network model and the intuition behind the high

level feature extraction. Section IV details the model implementation. Section V details the experimental analysis and Section VI concludes the paper with discussions related to future works.

II. RELATED WORK

Gesture recognition has drawn increasing attention of researchers, primarily due to its growing potential in areas such as robotics, human-computer interaction and user interface design. Different temporal models have been proposed. Nowozin and Shotton [36] proposed the notion of “action points” to serve as natural temporal anchors of simple human actions using a Hidden Markov Model. Wang *et al.* [37] introduced a more elaborated discriminative hidden-state approach for the recognition of human gestures. However, relying on only one layer of hidden states, their model alone might not be powerful enough to learn a higher level representation of the data and take advantage of very large corpus. In this paper, we adopt a different approach by focusing on deep feature learning within a temporal model.

There have been a few works exploring deep learning for action recognition in videos. For instance, Ji *et al.* [19] proposed using 3D convolutional neural network for automated recognition of human actions in surveillance videos. Their model extracts features from both the spatial and the temporal dimensions by performing 3D convolutions, thereby capturing the motion information encoded in multiple adjacent frames. To further boost the performance, they proposed regularising the outputs with high-level features and combining the predictions of a variety of different models. Taylor *et al.* [11] also explored 3D convolutional networks for learning spatio-temporal features for videos. The experiments in [34] show that multiple network averaging works better than a single individual network and larger nets will generally perform better than smaller nets. Providing there is enough data, averaging multi-column nets [17] applied to action recognition could also further improve the performance.

However, the advent of Kinect-like sensors has put more emphasis on RGB-D data for gesture recognition, but not only. For instance, the benefits of deep learning using RGB-D data have been explored for object detection or classification tasks. Dosovistskiy *et al.* [38] presented a generic feature learning for training a convolutional network using only unlabeled data. In contrast to supervised network training, the resulting feature representation is not class specific and are advantageous on geometric matching problems, outperforming the SIFT descriptor. Socher *et al.* [39] proposed a single convolutional neural net layer for each modality as inputs to multiple, fixed-tree RNNs in order to compose higher order features for 3D object classification. The single convolutional neural net layer provides useful translational invariance of low level features such as edges and allows parts of an object to be deformable to some extent. To address object detection, Gupta *et al.* [40] proposed a geocentric embedding for depth images that encodes height

above ground and angle with gravity for each pixel in addition to the horizontal disparity. This augmented representation allows CNN to learn stronger features than when using disparity (or depth) alone.

Recently, the gesture recognition domain itself has been stimulated by the collection of large public corpus. In particular, the ChaLearn LAP [41] gesture spotting challenge has collected around 14,000 gestures drawn from a vocabulary of 20 Italian sign gesture categories. The emphasis is on multi-modal automatic learning gestures performed by several different users, with the aim of performing user independent continuous gesture spotting. Some of the top winning methods in the ChaLearn LAP gesture spotting challenge require a set of complicated handcrafted features for either skeletal input, RGB-D input, or both. For instance, Neveroa *et al.* [42] proposed a pose descriptor consisting of 7 logical subsets for skeleton features while Monnier *et al.* [43] proposed to use 4 types of features for skeleton features (normalised joint positions; joint quaternion angles; Euclidean distances between specific joints; and directed distances between pairs of joints, based on the features proposed by Yao *et al.* [44]) and histograms of oriented gradients (HOG) descriptor for RGB-D images around hand regions. In [45], the state-of-the-art dense trajectory [9] handcrafted features are adopted for the RGB module.

There is a gradual trend to learn the features for gesture recognition in videos. For instance, the recent methods in [34], [35] focused on single modalities, used deep networks to learn representations from skeleton data [34] or from RGB-D data [35]. Neveroa *et al.* [42] presents a multi-scale and multimodal deep network for gesture detection and localisation. Key to their technique is a training strategy that exploits i) careful initialisation of individual modalities and ii) gradual fusion of modalities from the strongest to weakest cross-modality structure. One major difference compared to what we propose is the treatment of the time factor: rather than using a temporal model, they used frames within a fixed interval as the input of their neural networks for the prediction of the final gesture class, an approach that requires to train several multi-scale temporal networks to cope with gestures performed at different speeds. Furthermore, their skeleton features used in their network are sets of ad-hoc hand crafted features, rather than being learned from raw data.

III. MODEL FORMULATION & OVERALL APPROACH

Inspired by the framework successfully applied to speech recognition [20], the proposed model is a data driven learning system. This results in an integrated model, where the amount of prior knowledge and engineering is minimised. On top of that, this approach works without the need for additional complicated preprocessing and dimensionality reduction methods as it is naturally embedded in the framework.

The proposed approach relies on a Hidden Markov Model (HMM) for the temporal part, and neural networks to model the emission probabilities. In the remainder of this section, we will first present our

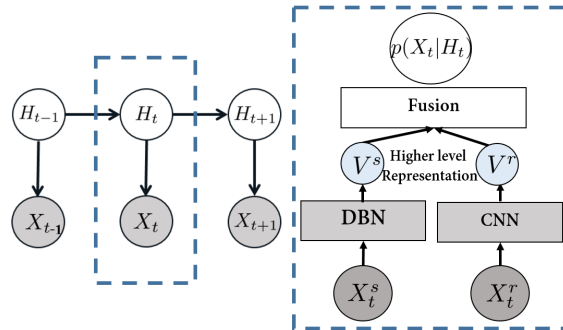


Fig. 1: Gesture recognition model: the temporal model is a HMM (left), whose emission probability $p(X_t|H_t)$ (right) is modeled by forward-linked neural networks. More precisely, observations X_t (skeletal features X_t^s , or RGB-D image features X_t^r) are first passed through appropriate deep neural nets (a Deep Belief Network - DBN- pretrained with Gaussian-Bernoulli Restricted Boltzmann Machines for the skeleton modality, and a 3D convolutional neural network -3DCNN- for the RGB-D modality) to implicitly extract high-level features (V^s and V^r) which are further fused to produce an estimate of $p(X_t|H_t)$.

temporal model and then introduce its main component. The details of the two distinct neural networks and fusion mechanisms along with post-processing will be provided in Section IV.

A. Deep Dynamic Neural Networks

The proposed deep dynamic neural network (*DDNN*) can be seen as an extension of [21], where instead of only using the restricted Boltzmann machines to model human motion, various connectivity layers (fully connected layers, convolutional layers) are stacked together to learn higher level features justified by a variational bound [14] from different input modules.

A continuous-observation HMM is adopted for modelling higher level temporal relationships. At each time step t , we have one observed random variable X_t composed of the skeleton input X_t^s and RGB-D input images X_t^r as shown in the graphical representation in Fig. 1. The hidden state variable H_t takes on values in a finite set \mathcal{H} composed of $N_{\mathcal{H}}$ states related to the different gestures. The intuition motivating the HMM model is that a gesture is composed of a sequence of poses where the relative duration of each pose may vary. This variance is captured by allowing flexible forward transitions within a Markov chain. In practice, H_t can be interpreted as being in a particular phase of a gesture a .

Classically under the HMM assumption, the joint probability of observations and states is given by:

$$p(H_{1:T}, X_{1:T}) = p(H_1)p(X_1|H_1) \prod_{t=2}^T p(X_t|H_t)p(H_t|H_{t-1}), \quad (1)$$

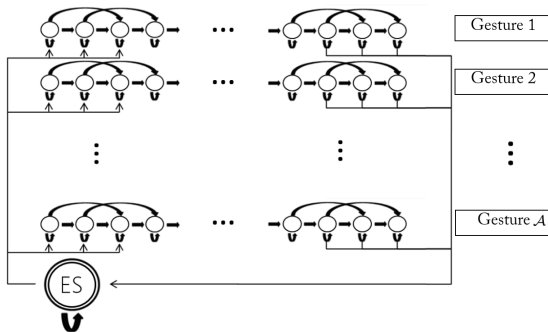


Fig. 2: State diagram of the *ES-HMM* model for low-latency gesture segmentation and recognition. An ergodic state (\mathcal{ES}) is used to model the resting position between gesture sequences. Each node represents a single state and each row represents a single gesture model. The arrows indicate possible transitions between states.

where $p(H_1)$ is the prior on the first hidden state, $p(H_t|H_{t-1})$ is the transition dynamics modelling the allowed state transitions and their probabilities, and $p(X_t|H_t)$ is the emission probability of the observation, modelled by deep neural networks in our case. These elements are presented below.

B. State-transition model and inference

The HMM framework can be used for simultaneous gesture segmentation and recognition. This is achieved by defining the state transition diagram as shown in Fig 2. For each given gesture $a \in \mathcal{A}$, a set of states \mathcal{H}_a is introduced to define a Markov model of that gesture. For example, for action sequence “tennis serving”, the action sequence can implicitly be dissected into $h_{a_1}, h_{a_2}, h_{a_3}$ as: 1) raising one arm 2) raising the racket 3) hitting the ball. More precisely, since our goal is to capture the variation in speed of the performed gestures, we set the transition matrix $p(H_t|H_{t-1})$ in the following way: when being in a particular node n at time t , moving to time $t+1$, we can either stay in the same node (slower), move to node $n+1$, or move to node $n+2$ (faster). Furthermore, to allow the segmentation of gestures, we add an ergodic state (\mathcal{ES}) which resembles the silence state for speech recognition and which serve as a catch-all state. From this state we can move to the first three nodes of any gesture class, and from the last three nodes of any gesture class we can move to \mathcal{ES} . Hence, the hidden variable H_t can take values within the finite set $\mathcal{H} = (\bigcup_{a \in \mathcal{A}} \mathcal{H}_a) \cup \{\mathcal{ES}\}$.

Overall, we refer to the model as the ergodic states hidden Markov model (*ES-HMM*) for simultaneously gesture segmentation and recognition. It differs from the firing hidden Markov model of [36] in that we strictly follow a left-right HMM structure without allowing backward transition, forbidding inter-states

transverse, assuming that the considered gestures do not undergo cyclic repetitions as in walking for instance.

Once we have the trained model, we can use standard techniques to infer online the filtering distribution $p(H_t|X_{1:t})$, or offline (or with delay) the smoothed distribution $p(H_t|X_{1:T})$ where T denotes the end of the sequence. Because the graph for the hidden Markov model is a directed tree, this problem can be solved exactly and efficiently using the max-sum algorithm also known as Viterbi algorithm. This algorithm searches the space of paths efficiently to find the most probable path with a computational cost that grows only linearly with the length of the chain [46]. The result of the Viterbi algorithm is a path-sequence $\hat{h}_{t:T}$ of nodes going through the state diagram of Fig.2 and from which we can easily infer the class of the gesture as illustrated in Fig. 8.

C. Learning the emission probability

Traditionally, emission probabilities for activity recognition have been trained with Gaussian Mixture Models (GMM), one per state. Alternatively, in this work we propose to model this term in a discriminative fashion. More precisely, since the input features have a high dimensionality, we propose to learn them using two distinctive types of neural networks suited to the input modality, as summarized in the right of Fig. 1.

Unfortunately, estimating a probability density such as an emission probability remains quite a difficult problem, especially in high dimensions. Theoretically, discriminative neural networks estimate posterior probabilities $p(H_t|X_t)$. We should divide posteriors by priors to get the scaled likelihoods which are required by the HMM for decoding. However, using scaled likelihood may not be beneficial if estimated priors do not match the priors in the test set [47]. Therefore, we employ the posteriors directly without dividing by the priors. This is equivalent to assuming that all priors are equal. or, in other words, inference in the HMM only depends only on the ratio between emission probabilities for the different states. One can interpret that the models are trained to directly predict the ratio between emission probabilities. This is similar to the approach used by Kindermans et al. to integrate transfer learning and an HMM based language model into a single probabilistic model [48]. One should think of the predicted emission probability ratio as an unnormalized version of the true emission probability. Nevertheless, to simplify the discussion of our models for readers with a basic understanding of HMMs, we will refer to the predicted emission probability ratio simply as emission probabilities since the underlying model remains unchanged.

For the skeletal features, we rely on a Deep-Belief Network (DBN) trained in two steps [49]: in the first step, stacked Restricted Boltzmann Machines (RBM) is trained in an unsupervised fashion using

only observation data to learn high-level feature representations; in the second step, the model is used as a Deep-Belief Network whose weights are further fine-tuned for learning the emission probability. For the RGB and depth (RGB-D) video data, we rely on a 3D (2D for space and 1D for time) convolutional neural networks (3DCNN) to model the emission probabilities. Finally, a fusion method combines in an intermediate or in a late stage the contributions of both modalities. In all cases (including the fusion), the supervised training is conducted by learning to predict the state label (an element of \mathcal{H}) associated to each training or testing frame.

Such an approach present several advantages over the traditional GMM paradigm. First, while GMMs are easy to fit when they have diagonal covariance matrices and, with enough components, can model any distribution, they have been shown to statistically inefficient at modeling high-dimensional features with many componential structure as explained in [20]. For instance, assume that the components of the input feature space can be separated into two subspaces characterized by N and M significantly different patterns in the training data, respectively, and that the occurrences of these patterns are relatively independent¹. A GMM will requires $N * M$ components to model this structure because each component must generate all the input features. On the other hand, a stacked RBMs model that can explains the data using multiple causes only requires $N + M$ components (in the ideal fully independent case), each of which is specific to a particular subspace. This exponential inefficiency of GMMs at modeling factorial structures leads to GMM+HMM systems having a very large number of Gaussians, most of which must be estimated from a very small fraction of the data.

Secondly, the approach for training the skeleton DBN model, first using variational learning to train stacked RBMs with unlabeled data, then in a discriminative fashion [49] has been shown to have several advantages. It has been observed that variational learning [14], which tries to optimize the data-likelihood while minizing the Kullback-Leibler divergence between the true posterior distribution of the hidden state (i.e. hidden layer variables of the RBMs in our case) and an approximation of this distribution, tends to produce unimodal distributions. This is beneficial, as this means that similar sensory inputs will be mapped to similar hidden variables. Thus, the intuition for using DBN for modeling the emission probability $p(X_t|H_t)$ from skeleton joints is that by learning the multi-layer network layer by layer, semantically meaningful high level features for skeleton configuration will be extracted while at the same time a parametric prior of human pose is learned. In our case, using the pair wise joints features as raw input, the data-driven approach network will be able to extract relational multi-joints features which are relevant to the target classes. For instance, from the “toss” action data, a wrist joints rotating

¹In our case, intuitively these spaces could be the features from different body parts, like left/right arm or torso features.

around shoulder joints feature is expected to be extracted from the backpropagation learning, and be the equivalent of those task specific *ad hoc* hard wired sets of joints configurations defined in [50] [51] [36] [52].

The benefit of such a learning approach is even more important when large amount of unlabelled data (e.g. skeleton data inferred from depth images of people performing unknown gestures) is available in addition to the labeled ones (this was not the case in this paper). Naturally, many of the features learned in this unsupervised way might be irrelevant for making the required discriminations, even though they are important for explaining the input data. However, this is a price worth paying if data availability and computation are cheap and lead to a stable mapping of the high-dimensional input into high-level features that are very good for discriminating between classes of interest. In this view, it is important to notice that each weight in a neural network is usually constrained by a larger fraction of the training samples than each parameter in a GMM, a point that has been masked by other differences in training. In particular, neural networks have traditionally been trained discriminatively, whereas GMMs are typically trained as generative models, which given their parametric nature partially compensate the fact that each mixture of a large GMM is usually trained on a very small fraction of the data.

In summary, the feed forward neural networks offer several potential advantages over GMMs:

- their estimation of emission probabilities does not require detailed assumptions about the data distribution;
- they allow an easy combination of diverse features, including both discrete and continuous features;
- they use far more of the data to constrain each parameter because the output on each training case is sensitive to a large fraction of the weights.

IV. MODEL IMPLEMENTATION

In this section, we detail the different component of the proposed Deep Dynamic Neural Network approach.

A. Ergodic States Hidden Markov Model

In all our experiments, the different modelling elements are specified as follows.

The number of states $N_{\mathcal{H}_a}$ associated to an individual gesture has been set to 5. Therefore, in total, the number of states is $N_{\mathcal{H}} = 20 \times 5 + 1 = 101$ when conducting experiments on the Chalearn dataset containing 20 classes. Note that intuitively, 5 states represents a good granularity as most gestures in the Chalearn are composed of 5 phases: an onset, followed by arm motions to reach a more static pose (often

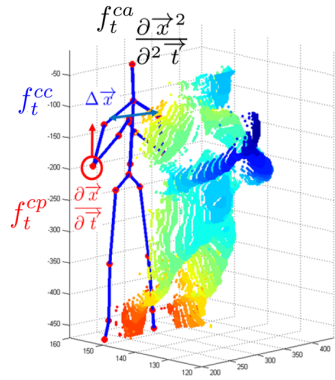


Fig. 3: Left: A point cloud projection of a depth image and the 3D positional features. Right: A DBN is trained to predict the emission probability $p(X_t^s|H_t)$ from the skeleton input f_t . The double arrows indicate that the intermediate weights are first trained in an unsupervised fashion using stacked RBMs.

characterized by a distinct hand posture), and the motion back to the rest place. In the future, optimal section of this number² and of different number of states per gesture could be investigated.

The training data in Chalearn is given as a set of sequences $\mathbf{x}_i = [x_{i,1}, \dots, x_{i,t}, \dots, x_{i,T_i}]$ where $x_{i,t} = [x_{i,t}^s, x_{i,t}^r]$ corresponds to the skeleton and RGB-D input. As only a single gesture label is provided for each sequence, we need to define $\mathbf{y}_i = [y_{i,1}, \dots, y_{i,t}, \dots, y_{i,T_i}]$, the sequence of state labels $y_{i,t}$ associated to each frame. To do so, a force alignment is used which means that if the i^{th} sequence is a gesture a , then the first $\lfloor \frac{T_i}{5} \rfloor$ frames are assigned to state h_a^1 (the first state of gesture a), the following $\lfloor \frac{T_i}{5} \rfloor$ frames are assigned to h_a^2 , and so forth.

Note that each gesture sequence comes with the video frames preceding and following the gesture. In practice, we extracted 5 frames before and after each gesture sequence and labelled them with the ergodic state (\mathcal{ES}) label. The transitional matrix $p(H_t|H_{t-1})$ was learned by simply collecting the transition statistics from the label sequences \mathbf{y}_i , allowing 5 frame jumps to accommodate skipping states.

B. Skeleton Module

1) *Skeleton input features:* Given our task, only the $N_j = 11$ upper body joints are relevant and considered, namely “*ElbowLeft*, *WristLeft*, *ShoulderLeft*, *HandLeft*, *ElbowRight*, *WristRight*, *ShoulderRight*, *HandRight*, *Head*, *Spine*, *HipCenter*”. The raw skeleton features of time t are defined as $x_t^s = [x_t^{s,1}, \dots, x_t^{s,N_j}]$. To capture the gesture dynamics, rather than using x_t^s as raw input to our data driven

²Experiments with 10 states led to similar performance.

approach, we follow the approach of [21] and compute the 3D positional pairwise differences of joints as well as temporal derivatives, defined as (as shown in Fig. 3) ³:

$$f_t^{cc} = \{x_t^{s,i} - x_t^{s,j} | i, j = 1, 2, \dots, N_j; i \neq j\} \quad (2)$$

$$f_t^{cp} = \{x_{t+1}^{s,i} - x_t^{s,i} | i = 1, 2, \dots, N_j\} \quad (3)$$

$$f_t^{ca} = \{x_{t+1}^{s,i} - 2 \times x_t^{s,i} + x_{t-1}^{s,i} | i = 1, 2, \dots, N_j\} \quad (4)$$

This results in an input feature vector $\mathbf{f}_t = [f_t^{cc}, f_t^{cp}, f_t^{ca}]$ of dimension $N_f = N_j \times (\frac{N_j}{2} + N_j + N_j) * 3 = 891$. Admittedly, here we do not completely neglect human prior knowledge about information extraction for relevant static postures, velocity and acceleration of overall dynamics of motion data. While we have indeed used prior knowledge to define our relevant features, we believe they remain quite general and do not need dataset specific tuning. Note that the feature extraction process resembles the computation of the *Mel Frequency Cepstral Coefficients (MFCCs)* and their temporal derivatives typically used in the speech recognition community [20].

2) *Modeling X_t^s using Deep Belief Networks:* Given the input skeleton feature \mathbf{f} , a *DBN* model is used to predict the emission probability, as shown in Fig. 3. As explained in Section III-C, the learning proceeds in two steps: in the first one, the network is considered as a stack of RBMs, and trained using a greedy, layer-by-layer unsupervised learning algorithm [14]; in the second one, a softmax network layer is added on top of the RBMs to create a *DBN* architecture, where the weights of the first step are used to initialize the corresponding weights in the *DBN*, and the *DBN* is further trained and fine-tuned in a supervised fashion to predict the emission probability. The number of nodes at each layer of the *DBN* are $[N_f, 2000, 2000, 1000, N_H]$. We provide below further details on the model and training.

Gaussian-Bernoulli RBM. Restricted Boltzmann machine (RBM) are undirected graphical models involving visible and hidden variables, with symmetric connections between the hidden and visible units but no connection within hidden variables or visible variables. In most cases, RBMs rely on binary random variables. However, in our case the visible unit in the first layer are the vector of skeleton features $\mathbf{f} \in \mathbf{R}^{N_f}$, which are continuous. To account for this situation, we thus resort to a Gaussian-Bernoulli RBM (*GRBM*) [49], whose main difference w.r.t. standard RBM lies in the following: the energy term of our first layer \mathbf{f} to the hidden binary stochastic units $\mathbf{h} \in \{0, 1\}^F$ is given by:

$$E(\mathbf{f}, \mathbf{h}; \theta) = - \sum_i \frac{(f_i - b_i)^2}{2\sigma_i^2} - \sum_i \sum_j W_{ij} h_j \frac{f_i}{\sigma_i} - \sum_{j=1} a_j h_j \quad (5)$$

³Note that the offset features used in [21] depend on the first frame. Thus if the initialisation fails which is a very common scenario, the feature descriptor will be generally very noisy. Hence, here we do not use these offset features.

where $\theta = \{W, b, a\}$ are the free parameters: $W_{i,j}$ serves as the symmetric synergy term between visible unit i and hidden unit j , while b_i and a_j are the bias term of the visible and hidden units, respectively. The conditional distributions needed for inference and generation are given by the traditional logistic function g for the binary hidden variable, and the normal distribution \mathcal{N} for the continuous variable:

$$P(h_j = 1|\mathbf{f}) = g\left(\sum_i W_{ij} f_i + a_j\right) \quad (6)$$

$$P(f_i = f|\mathbf{h}) = \mathcal{N}(f|\mu_i, \sigma_i^2). \quad (7)$$

where $\mu_i = b_i + \sigma_i^2 \sum_j W_{ij}$. In practice, we normalise the data (mean subtraction and standard deviation division) in the preprocessing phase. Hence, instead of learning σ_i^2 , one typically used $\sigma_i^2 = 1$ during training.

We ran 100 epochs using a fixed recipe based on stochastic gradient descent with a mini-batch size of 200 training cases to train the stacked RBM, in which the learning rate is fixed at 0.001 for the Gaussian-Bernoulli RBMs, and at 0.01 for the following binary-binary RBMs.

DBN forward training. The DBN is initialized with the result of the previous step, a method which tends to avoid suboptimal local minima and increase the networks performance stability. The learning rate for the parameter fine tuning starts at 1 with 0.99999 mini-batch scaling. During the experiments, early stopping occurs around epoch 440. The optimisation completes with a frame based validation error rate of 16.5%.

C. RGB & Depth 3D Module

1) *Preprocessing:* Although DeepMind technology [53] presented the first deep learning model to successfully learn control policies directly from high-dimensional sensory input using deep reinforcement learning, working directly with raw input Kinect recorded data frames, which are 640×480 pixel images, can be computationally demanding. Therefore, our first step in the preprocessing stage consists of cropping the highest hand and the upper body using the given joint information. In the Chalearn dataset, we determined that the highest hand is the most interesting. When both hands are used, they normally perform the same (mirrored) movement, and when one hand is used, it is always the highest one which is relevant. Furthermore, to be invariant to handedness, we always train the model with the right hand view. That is, when the left hand is actually the performing hand, the video was mirrored.

The preprocessing results in four video samples (body and hand with grayscale and depth) of resolution 64×64 . Furthermore, the noise in the depth maps is reduced by removing the background using the automatically produced segmentation mask provided with the data, and applying a median filtering. Depth

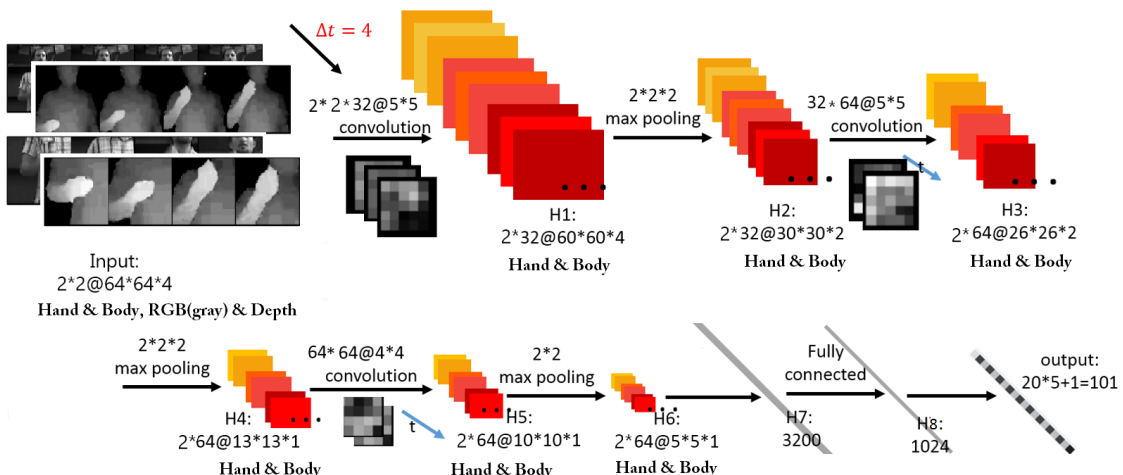


Fig. 4: 3DCNN architecture. The input is $2 \times 2 @ 64 * 64 * 4$, meaning 2 modalities (depth and RGB) for the hand and body regions, each being 4 consecutive 64 by 64 frames stacked together. See text for further details.

images are Z-normalised (the mean is subtracted -as it is rather irrelevant to the gesture subclass- and the result divided by the standard deviation), whereas RGB images are only normalized by the image standard deviation. The outcome is illustrated in Fig. 5.

2) *3DCNN Architecture*: This architecture consists of a series of layers composed of either convolution, pooling or, in the last layer, fully connected layers. The 3D convolution itself is achieved by convolving a 3D kernel to the cuboid formed by stacking multiple contiguous frames together. We follow the nomenclature of in [19]. However, instead of using *tanh* units [19], Rectified Linear Units (*ReLUs*) [16] were used in order to speed up training. Formally, the value of a unit at position (x, y, z) (z here corresponds to the time-axis) in the j -th feature map in the i -th layer, denoted as v_{ij}^{xyz} , is given by:

$$v_{ij}^{xyz} = \max(0, (b_{ij} + \sum_m \sum_{p=0}^{P_i-1} \sum_{q=0}^{Q_i-1} \sum_{r=0}^{R_i-1} w_{ijm}^{pqr} v_{(i-1)m}^{(x+p)(y+q)(t+r)})) \quad (8)$$

The complete 3DCNN architecture is depicted in Fig. 4: 4 types of input contextual frames are stacked as size $64 \times 64 \times 4$ (as illustrated in Fig. 5). The first layer (H1) consists of 32 feature maps produced by 5×5 spatial convolutional kernels, followed by local contrast normalisation (LCN) [54]. Note that the filter response maps of the Depth and RGB images of the hand (and body) are summed to produce a single feature map, thus resulting in H1 in 32 feature maps for each of the hand and for the body region. A 3D max pooling with strides (2, 2, 2) is then applied. The second layer uses 64 feature maps with 5×5 kernels followed by LCN and 3D max pooling with strides (2, 2, 2). The third layer is composed

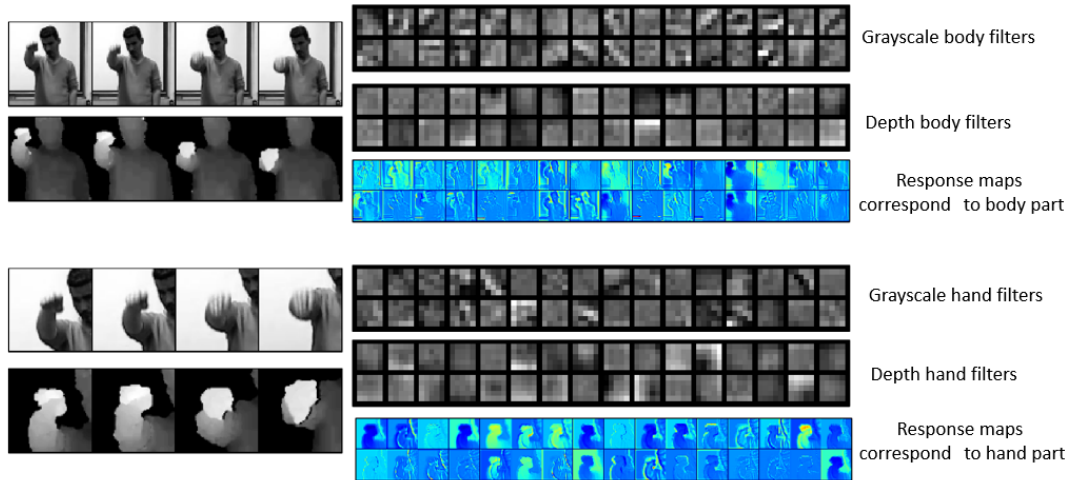


Fig. 5: Visualisation of input frames, first convolutional layer 5×5 filters, and corresponding response maps. As depth images are smoother than the grayscale ones, the corresponding filter are smoother as well.

of 64 feature maps with 4×4 kernels followed by 3D max pooling with strides (1, 2, 2). All hand and body convolutional layer outputs of H6 are flattened in H7, and fed into one fully connected layer of size 1024. Finally, the output layer has N_H values, the number of states in the HMM state diagram (see Fig. 2).

3) *Details of Learning:* During training, dropout [55] is used as main regularisation approach to reduce overfitting. Nesterovs accelerated gradient descent (NAG) [56] with a fixed momentum-coefficient of 0.9 and mini-batches of size 64 are also used. The learning rate is initialised at 0.003 with a 5% decrease after each epoch. The weights of the 3DCNNs are randomly initialised with a normal distribution with $\mu = 0$ and $\sigma = 0.04$. The frame based validation error rate is 39.06% after 40 epochs. Compared with the skeleton module (16.5% validation error rate), the 3DCNN has a notable higher frame based error rate.

4) *Looking into the Networks: visualisation of Filter Banks:* The convolutional filter weights of the first layer are depicted in Fig. 5. The unique characteristics from the kernels are clearly visible: as hand input images (RGB and depth) have larger homogenous areas than the body inputs, the resulting filters are smoother than their body counterpart. In addition, while being smoother overall than the grayscale filters, depth filters exhibit stronger edges, as also reported in [39]. Finally, by looking at the joint depth-image response maps, we can notice that some filters better capture segmentation like information, while other are more edge oriented.

1
2
3 *D. Multimodal Fusion*
4
5

6 To combine the two modalities, two strategies can be used, as shown in Fig. 6: a late fusion approach
7 and an intermediate fusion approach.
8
9

10 *1) Late Fusion:* This scheme fuses the combination of the emission probabilities estimated from the
11 different input. While different combinatin schemes exist, here we considered a simple linear combination:
12
13

$$\log p(X_t|H_t) \propto \alpha \cdot \log p(X_t^s|H_t) + (1 - \alpha) \cdot \log p(X_t^r|H_t) \quad (9)$$

14 where the different emission probabilities are provided by the modules described in IV-B and IV-C, and
15 α is a coefficient that controls the contributions of each source of information and which is estimated by
16 cross validation. Interestingly, the best performing α is close to 0.5, indicating that both modalities are
17 equally important.
18
19

20 *2) Intermediate Fusion:* As an alternative to the late fusion scheme, we can take advantage of the
21 high-level representation implicitly learned by each module (and represented by the V^s and V^r nodes
22 of the penultimate layer of the respective networks, before the softmax) to fuse the modality in an
23 intermediate fashion by concatenating these two layers in one layer of 2024 hidden unites and learning
24 a cross-modality emission probability predictive network. Note that this is very similar in spirit to the
25 approach proposed in [22] for audio-visual speech recognition. An important difference is that in [22],
26 the same stacked RBMs/DBN architecture was used to represent both modalities before fusion, whereas
27 in our case, a stacked RBMs/DBN and a 3DCNN are used. Also, [22] proposed the use of a multimodal
28 autoencoder to handle predictions when potentially only one modality migth be present, a point that we
29 do not address.
30
31

32 The resulting architecture is trained by first initializing the weights of the deeper layers from the
33 previously trained module, and then jointly fine tuning the whole network (including learning the last
34 layer parameters) and stop the training when the validation error rate stops decreasing (~ 15 epochs). We
35 argue that using the “pre-trained” parameters is important due to the heterogeneity of the inputs of the
36 system, and that the joint training should adjust parameters to handle this heterogeneity and produce the
37 final estimates.
38
39

40 V. EXPERIMENTS AND ANALYSIS
41
42

43 This Section reports the experiments performed to validate our model. First, we will introduce the
44 ChaLearn dataset, and then present the experimental protocol we followed. In Section V-C, we will present
45 and analyse the obtained results, including a discussion on the modeling elements. Finally, Section V-D
46 will briefly discuss the computational complexity of the approach.
47
48

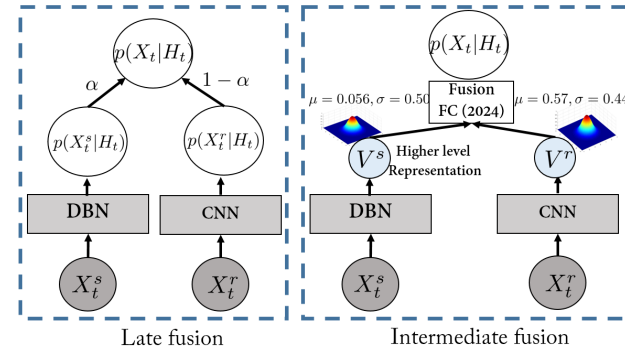


Fig. 6: Multimodal dynamic networks with late fusion scheme (left) and intermediate fusion scheme (right). The late approach simply combines the emission probabilities from two modalities. In the intermediate fusion scheme, each modality (skeleton and RGB-D) is first pre-trained separately, and their high-level representation V^s and V^r (the penultimate node layers of their neural networks) are concatenated to generate a shared representation. The resulting architecture is trained jointly.

A. Chalearn LAP Dataset

The dataset used in this work is provided by the ChaLearn LAP [41] gesture spotting challenge⁴. The focus is on “multiple instance, user independent spotting” of gestures, which means learning to recognize gestures from several instances for each category performed by different users, drawn from a gesture vocabulary of 20 Italian cultural/anthropological signs. A gesture vocabulary is a set of unique gestures, generally related to a particular task.

The challenge dataset contains 940 video sequences, each performed by a single person and composed of 10 to 20 gesture instances for a total of around 14,000 gestures. There are 20 gesture classes, *i.e.* *vattene*, *vieniqui*, *perfetto*, *furbo*, *cheduepalle*, *chevuoi*, *daccordo*, *seipazzo*, *combinato*, *freganiente*, *ok*, *cosatifarei*, *basta*, *prendere*, *noncenepiu*, *fame*, *tantotempo*, *buonissimo*, *messidaccordo*, *sonostufo*, with a number of samples well balanced between classes. The average length of gestures is 39 frames, the minimum frame number for a gesture is 16 and the maximum frame number is 104.

This dataset is challenging because the “user independent” setting and some of gestures differ primarily in hand pose but not the overall arm motions as illustrated in Fig. 7. In terms of data, three modalities are provided with the input videos: the sequence of skeleton joints, and the RGB and depth images (including a segmentation of the person performing the gesture).



Fig. 7: Examples of gestures in the ChaLearn dataset. This dataset is challenging because the “user independent” setting (a)&(b), some of gestures differ primarily in hand pose but not the overall arm motions (d)&(e) and some gestures require both hands to perform (g,h,i). Subtle hand movement (c) and differences in performing speed and range (f) also make recognising tasks challenging.

B. Experimental protocol

1) *Training and evaluation protocol:* We follow the ChaLearn experimental protocol, in which the input sequences are split into 700 videos for training, and 240 sequences for testing and reporting results. Note that the test sequences are not segmented a priori and the gestures must be detected within a continuous data stream which, in addition to the targeted gestures, also contains noisy and out-of-vocabulary gestures. Furthermore, in the experiments, we split the training videos into 650 videos for learning the actual neural network model parameters, and 50 videos used as validation data for monitoring the training performance or selecting hyper-parameters.

2) *Performance measures:* Several measures can be used to evaluate the gesture recognition performance. In this work, we adopted the ChaLearn performance measure known as the Jaccard index, which

⁴<http://gesture.chalearn.org/2014-looking-at-people-challenge/data-2014-challenge>

1
2
3 relies on a frame-by-frame prediction accuracy. More precisely, if GT_i denotes the sequence of ground
4 truth labels in video i , and R_i the algorithm output, the Jaccard index of the video is defined as:
5

$$JI_i(GT_i, R_i, g) = \frac{N_s(GT_i, R_i, g)}{N_u(GT_i, R_i, g)}, \quad (10)$$

$$\text{and } JI_i = \frac{1}{|\mathcal{G}_i|} \sum_{g \in \mathcal{G}_i} JI_i(GT_i, R_i, g) \quad (11)$$

12 where $N_s(GT_i, R_i, g)$ denotes the number of frames where the ground truth and result agree on the
13 gesture class g , and $N_u(GT_i, R_i, g)$ denotes the number of frames labeled as a gesture frame g by either
14 the ground truth or the algorithm, and \mathcal{G}_i denotes the set of gestures either in the ground truth or detected
15 by the algorithm in sequence i ⁵. The average of the JI_i over all test videos is reported as performance
16 measure. Note that experimentally, this measure tends to favours having more false positives than missing
17 true positives, in order to increase the numerator.
18

19 Being defined at the frame level, the Jaccard index can vary due to variations of the segmentation (both
20 in the ground truth and recognition) at gesture boundaries, which can be irrelevant from an application
21 viewpoint. Thus, we also defined performance at the gesture event level by following the commonly used
22 PASCAL challenge intersection over union criterion. More precisely, if for a gesture segment G , we have
23 $\frac{G \cap R}{G \cup R} > 0.5$, where R denotes a recognized gesture segment of the same class, then the gesture is said to
24 be recognized. If the same relation holds but with a gesture segment of another class, the prediction is
25 incorrect. Otherwise the gesture is rated as undetected. This allows us to define the *Recognized*, *Confused*
26 and *Missed* performance measures at the video level, which are further averaged over test sequences for
27 reporting.
28

29 *3) Tested systems:* We evaluated the recognition performance made by the HMM applied to the
30 emission probabilities estimated from either the skeleton data, the RGB-D image data, the late fusion
31 scheme, and the intermediate fusion scheme. Note that in all cases the HMM output was further filtered
32 to avoid false alarms, by considering gesture segments of less than 20 frames as noise and discarding
33 them.
34

35 C. Results

36 **Overall results.** The overall performance of the algorithms are given in Tables I and II. As can be
37 observed from both performance measures, the skeleton module usually performs better than the RGB-D
38 module. In addition, its generalization capability is better than that of the RGB-D module, especially when
39

40
41
42
43
44
45
46
47
48
49
50
51
52
53
54
55
56
57
58
59
60
5^{Note} that 'non gesture' frames are thus excluded from the counts.

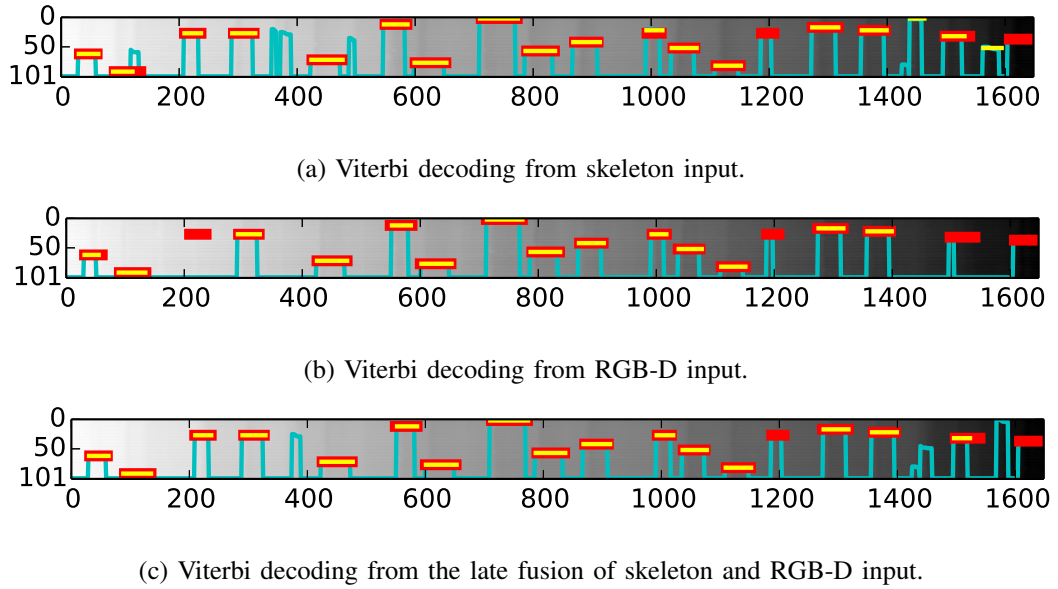


Fig. 8: Viterbi decoding of sample sequence #700, using skeleton (top), RGB-D (middle) and late fusion system (bottom). The x-axis represents time and the y-axis represents the hidden states of all classes and of the ergodic state (state 101). The cyan lines represent the viterbi shortest path, while red lines denote the ground truth labels, and the yellow segments are the predicted labels. The fusion method exploits the complementary properties of individual modules, e.g. around frame 200 the skeleton help solving the missed detection from the 3DCNN module, while around frame 1450, the 3DCNN module can help suppress the false positive prediction made by the skeleton module.

Module	Validation	Test
Skeleton – DBDN	0.783	0.779
RGB-D – 3DCNN	0.752	0.717
Multimodal Late Fusion	0.817	0.809
Multimodal Inter. Fusion	0.800	0.798

TABLE I: Results in terms of Jaccard index JI for the different network structures and modalities modeling the emission probabilities.

measured with the Jaccard index where there is almost no drop of performance between the validation and test data. One possible explanation is that the information in the skeleton data is more robust, as it benefited from training using huge and highly varied data [24]: around one million images from both realistic and synthetic depth images were used to train the decision forest classifiers involved in the joints extraction. On the other hand, as the RGB-D module relies on the raw data and was learned only from the ChaLearn training set, it may suffer from some overfitting. Another interesting conclusion that can

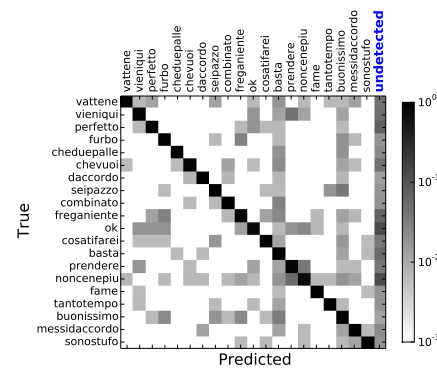
	%	Validation	Test
Skeleton - DBDN	<i>Recognized</i>	86.3	83.6
	<i>Confused</i>	11.4	12.3
	<i>Missed</i>	2.3	4.1
RGB-D - 3DCNN	<i>Recognized</i>	78.7	75.8
	<i>Confused</i>	5.2	4.5
	<i>Missed</i>	16.1	19.7
Multimodal Late Fusion	<i>Recognized</i>	87.9	86.4
	<i>Confused</i>	9.1	8.7
	<i>Missed</i>	3.0	4.9
Multimodal Inter. Fusion	<i>Recognized</i>	86.5	85.5
	<i>Confused</i>	7.3	6.8
	<i>Missed</i>	6.2	7.7

TABLE II: Gesture classification performance at the event level, in percentage of the number of ground truth gestures.

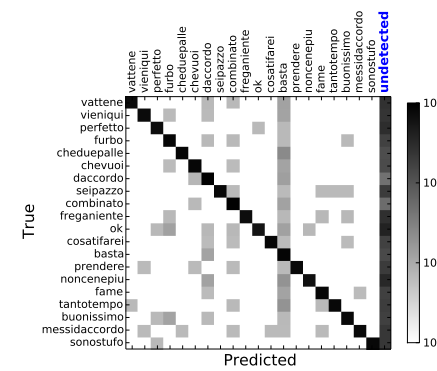
be drawn from Table II is that while most errors from the RGB-D module are due to under detection (the *Missed* rate is 19.7%, whereas it is only 4.1% for the skeleton), the skeleton module is more reactive to gesture activity, but makes more mistakes (the *Confused* rate is 12.3% vs 4.5% for RGB-D).

Finally, the results also demonstrate that the combination of both modalities is more robust, as shown by the recognition rate increase and the smaller drop in the generalization performance (for instance the decrease of the *Recognized* rate is lower than for the skeleton data alone).

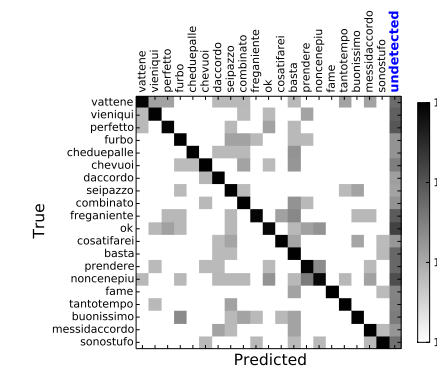
Confusion matrices. The confusion matrices (in log-form) in Fig. 9 better illustrate the complementarity of the behaviors of the two modalities. The higher underdetection of RGB-D is clearly visible (whiter matrix, except last 'undetected' column). We can also notice that some gestures are more easily recognized than others, or catch the difficult instances of other gestures. This is the case of the "Basta" gesture, whose arms motion resembles the start and end of the arm motion of many other gesture (see Fig. 7). Whatever the modality, its model thus tends to recognize few instance of all other gesture classes, whenever their likelihood are low when being evaluated using the HMM states associated with their true label due to too much variability. Similarly, the hand movement and pose of the "Buenissimo" gesture is present in several other gesture classes, whose instances are then often confused with "Buenissimo" when relying on the skeleton information alone. However, as these gestures differ primarily in their hand pose, such confusion is much more reduced using the RGB-D domain, or when fusing the skeleton and RGB-D modules. The complementary properties of the two modalities is also illustrated from the Viterbi path



(a) Skeleton - DBN



(b) RGB-D - 3DCNN



(c) Multimodal Late Fusion

Fig. 9: Confusion Matrices (log-norm) for the different modalities.

decoding plot in Fig. 8. In general, the benefit of this complementarity between arm pose/gesture and hand pose can be observed from the whiter confusion matrix than in the skeleton case (less confusion due to hand pose information from RGB-D) and much less under-detection than in the RGB-D case (better

1
2
3 upper-body pose discrimination thanks to skeleton input).

4
5 However, the modalities by themselves have more difficulties to correct the recognition errors which
6 are due to variations coming from the performer, like differentiating people that gesticulate more (see
7 Fig. 11).

8
9
10
11
12
13
14
15
16
17
18
19
20
21
22
23
24
25
26
27
28
29
30
31
32
33
34
35
36
37
38
39
40
41
42
43
44
45
46
47
48
49
50
51
52
53
54
55
56
57
58
59
60
Late vs. Intermediate fusion. The results in Tab. I and II show that the intermediate fusion system improved individual modalities, but without outperforming the late fusion system. The result is counter-intuitive, as we would have expected the cross-modality learning in the intermediate fusion scheme to result in better emission probability predictions, as compared to the simple score fusion in the late system. One possible explanation is that the independence assumption of the late scheme better preserves both the complementarity and redundancy of the different modalities, properties which are important for fusion. Another related explanation is that in the intermediate fusion learning process, one modality may dominate and skew the network towards learning that specific module and lowering the importance of the other one. The large difference between the mean activations of the skeleton module neurons which are predominantly larger than those of the RGB-D ConvNet's (0.57 vs. 0.056) can be an indicator of such a bias during the multimodal fine-tuning phase and support this conjecture, even if these mean activations are not directly comparable due to the neuron heterogeneity (the skeleton DBN has logistic units whereas the 3DCNN ConvNet has relu units). Note that such heterogeneity was not present when fusing modalities in [22], where better registration and less spatial registration variability in lip images allowed to also resort to the same stacked RBMs for the visual modality (rather than 3DCNN) and the audio one. More investigation on how to handle heterogeneous networks should be conducted.

61
62
63
64
65
66
67
68
69
70
71
72
73
74
75
76
77
78
79
80
81
82
83
84
85
86
87
88
89
90
91
92
93
94
95
96
97
98
99
100
HMM benefit. As the emission probabilities are learned in a discriminative manner, one could wonder whether the HMM brings benefit beyond smoothing. To investigate this issue, we removed the temporal structure as follows: for a given gesture \mathbf{a} , we computed its score at time t , $Score(\mathbf{a}, t)$, by summing the emission probabilities $p(X_t | H_t = h)$ for all nodes associated to that gesture, i.e. $h \in \mathcal{H}_\mathbf{a}$. This score is then smoothed in the temporal domain (using a window of 5 frames) to obtain $\widehat{Score}(\mathbf{a}, t)$. Finally, following [57], the gesture recognition proceeds in two steps: first finding gesture segments by thresholding the score of the ergodic state; then, for each resulting gesture segment, the recognized gesture is defined as the one whose average score within the segment is the highest. Fig. 10 illustrates this process along with the DDNN and ground-truth. In general, we could observe that better decisions on the presence of gestures and on the boundaries where a gesture starts and ends are achieved with the proposed *DDNN* thanks to the use of the state-diagram defined in Fig. 2, as compared to the above method, where deciding on a gesture detection threshold is rather unstable and quite sequence dependent.

Module	Skeleton	RGB-D	Fusion
[43] 3 set skeletal & HOG, Boosted classifier	0.791	-	0.822
[59] 3D skeletal pose & HOG, MRF	0.790	-	0.827
[45] Dense trajectory (HOG, HOF, MBH)	-	0.792	-
[58] Template based Random Forest Classifier	-	-	0.747
[60] Fisher Vector, Dynamic Programming	0.745	-	-
[61] Independent Subspace Analysis, RF	-	0.649	-
[62] PHOG, SVM, HMM	0.454	0.462	0.597
[42] Representation Learning (multiscal)	0.808	0.809	0.849
[35] CNN	-	0.789	-
[34] Deep Neural Networks	0.747	0.637	0.804
DDNN (this work)	0.779	0.717	0.809

TABLE III: Comparison of results in terms of the ChaLearn Jaccard index with state-of-the-art related works.

Indeed, the overall performance of the above scheme without the HMM temporal sequencing is reduced to $JI = 0.66$, while the *Recognized*, *Confused* and *Missed* corresponding to Table II for the test set are 76.6 , 5.3 and 18.1. However, note that the above method relying on only the gesture probability learned using neural networks on 5 frame inputs still outperforms the Jaccard index of 0.413 obtained by [58] when using a 5 frames template matching system where all the features are handcrafted.

Comparison with the state-of-the-art. The performance of recent state-of-the-art techniques is given in Table III. The first half of the table resort to hand crafted feature approaches and then usually a second stage classifier. Our proposed system performs on par with the top two methods. However, hand crafted feature methods' performance are saturated regardless of the increase training data. The representation learning methods in the second half of the Table perform comparably with the best hand crafted feature approaches and the top representation method achieves the best Jaccard index score. Given more training data, it is expected that the networks will be able to be more adapted to the “user independent” setting. It also worths noting that our proposed system is the only method that incorporates the temporal modelling element rather than sliding window approach. We believe this is an interesting research direction that can be more adapted to various lengths of gestures and relevant temporal factors.

D. Computational Complexity

We can distinguish between two complexities: the training one, and the test one.

Complexity at training time. Although training deep neural network using stochastic gradient descent is

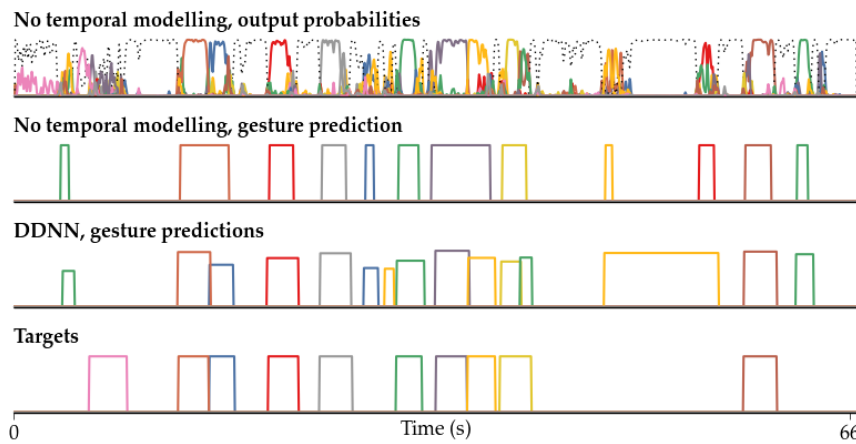


Fig. 10: HMM temporal contribution. First row: output emission probabilities for each gesture as given by the late fusion scheme (see text) for the test set #703. The dashed line represents the probability of the Resting/Other gesture state, while other colour represent different gestures. Second row: resulting recognized gestures, without HMM modeling. Third row: HMM output. Fourth row: ground truth segmentation. Without temporal modelling, the decision boundary of a gesture will be more rugged and it is more difficult to make hard decisions of where the gesture starts or ends. Hence, in general, it causes miss-detection and miss-merging. Thanks to the HMM temporal modelling and Viterbi path decoding, gesture boundaries are usually cleaner defined from the Resting state to the gesture states, resembling the behavior of the manual annotators with better accuracy.

computationally intensive, the reuse of pre-trained network parameters as done in our case can help with better initialisation and lead to faster convergence. We can observe different training time in function of the modality (and architecture). Specifically, using a modern GPU (GeForece GTX TITAN Black) and conv op. by Theano [63], the training time of each epoch of the DBN skeleton module is less than 300 seconds and allows training the required 500 epochs within 2 days. The training time of each epoch of the 3DCNN RGB-D module is much more expensive, taking more than 10,000 seconds. Hence, 40 epochs takes around 5 days to train. The fusion network being initialised with the individual module parameters, its training time is half that of the 3DCNN.

Complexity at test time. Given the learned models, our framework with the above GPU can perform real-time video sequence labelling with a low inference cost. More specifically, a single feed forward neural network incurs linear computational time ($\mathcal{O}(T)$), and is efficient because it requires only matrix products and convolution operations. The complexity of the Viterbi algorithm is itself of $\mathcal{O}(T * |S|^2)$, where T is the number of frames and $|S|$ the number of states, and thus performs real-time given our state-space. In practice, our multimodal neural network can be deployed at 90 FPS. The preprocessing



(a) Sample #806



(b) Sample #702

Fig. 11: Examples of performer variations in the upper body dynamic. Most performers tend to keep their upper-body static while performing the gesture, leading to good recognition performance (Jaccard index of person on the top is 0.95 for the late fusion system). Some persons are more involved and move more vehemently (person at the bottom, Jaccard index of 0.61), which can affect the recognition algorithm itself (bottom left samples) or even the skeleton tracking (bottom right; note that normally cropped images are centered vertically on the head position).

part takes most of the time and our un-optimized version runs at 25 FPS, while the Viterbi decoding runs at 90 FPS. Hence, the overall system can achieve faster than real-time performance.

VI. CONCLUSION AND FUTURE WORK

Hand-engineered, task-specific features are often task-specific and time-consuming to design. This difficulty is even more pronounced with multimodal data as we would like the features to relate to multiple data sources. In this paper, we presented a novel deep dynamic neural network (DDNN) for learning contextual frame-level representations and modelling emission probabilities in the framework of an HMM temporal model. Different feature learning methods (DBN and 3DCNN) suited to the heterogeneous inputs from skeletal joints, RGB images, and depth images were proposed, as well as different fusion schemes. Experimental results on bi-modal gesture time series show that the multimodal DDNN framework can learn good models of the joint space of multiple sensory inputs, improving over unimodal input.

There are several directions for future work. Our results with those of other recent works suggest that learning features directly from data is a very important research direction and that with more and more data and flops-free computational power, learning-based methods are not only more generalisable to many domains, but also are powerful in combination with other well-studied probabilistic graphical models for dynamical modelling and reasoning. In this view, the learning of better shared and complementary representation among multimodal and heterogeneous inputs, as done in [57], requires more exploration. In addition, while the proposed HMM provided a good basis for the temporal modeling of gestures, other

more discriminant temporal approaches such as Conditional Random Field or further and better variants [37] could be directly exploited at their advantage in conjunction with our deep neural network learning approach. Ultimately, in a logical way, these two research directions converge into the investigation of a single and unified deep learning framework fusing heterogeneous modalities by using recent Recurrent Neural Networks such as Long Short Term Memory [64] for modelling the temporal component of the problem.

APPENDIX A

DETAILS OF THE CODE

The python code using Theano [63] for this work can be found at:

https://github.com/stevenwudi/chalearn2014_wudi_li

ACKNOWLEDGMENT

The authors would like to thank Sander Dieleman for his guidance in building, training and initialising convolutional neural networks.

REFERENCES

- [1] L. Liu, L. Shao, F. Zheng, and X. Li, "Realistic action recognition via sparsely-constructed gaussian processes," *Pattern Recognition*, doi: 10.1016/j.patcog.2014.07.006., 2014.
- [2] L. Shao, X. Zhen, and X. Li, "Spatio-temporal laplacian pyramid coding for action recognition," *IEEE Transactions on Cybernetics*, vol. 44, no. 6, pp. 817-827, 2014.
- [3] D. Wu and L. Shao, "Silhouette analysis-based action recognition via exploiting human poses," *IEEE Transactions on Circuits and Systems for Video Technology*, vol. 23, no. 2, pp. 236-243, 2013.
- [4] I. Laptev, "On space-time interest points," *International Journal of Computer Vision*, 2005.
- [5] P. Dollár, V. Rabaud, G. Cottrell, and S. Belongie, "Behavior recognition via sparse spatio-temporal features," in *Visual Surveillance and Performance Evaluation of Tracking and Surveillance*. IEEE, 2005.
- [6] G. Willems, T. Tuytelaars, and L. V. Gool, "An efficient dense and scale-invariant spatio-temporal interest point detector," in *European Conference on Computer Vision*. Springer, 2008.
- [7] P. Scovanner, S. Ali, and M. Shah, "A 3-dimensional sift descriptor and its application to action recognition," in *International Conference on Multimedia*. ACM, 2007.
- [8] A. Klaser, M. Marszalek, and C. Schmid, "A Spatio-Temporal Descriptor Based on 3D-Gradients," in *British Machine Vision Conference*, 2008.
- [9] H. Wang, A. Kläser, C. Schmid, and C.-L. Liu, "Dense trajectories and motion boundary descriptors for action recognition," *International Journal of Computer Vision*, 2013.
- [10] H. Wang, M. M. Ullah, A. Kläser, I. Laptev, C. Schmid *et al.*, "Evaluation of local spatio-temporal features for action recognition," in *British Machine Vision Conference*, 2009.
- [11] G. W. Taylor, R. Fergus, Y. LeCun, and C. Bregler, "Convolutional learning of spatio-temporal features," in *European Conference on Computer Vision*. Springer, 2010.

- [12] Q. V. Le, W. Y. Zou, S. Y. Yeung, and A. Y. Ng, "Learning hierarchical invariant spatio-temporal features for action recognition with independent subspace analysis," in *IEEE Conference on Computer Vision and Pattern Recognition*, 2011.
- [13] M. Baccouche, F. Mamalet, C. Wolf, C. Garcia, and A. Baskurt, "Spatio-temporal convolutional sparse auto-encoder for sequence classification," in *British Machine Vision Conference*, 2012.
- [14] G. E. Hinton, S. Osindero, and Y.-W. Teh, "A fast learning algorithm for deep belief nets," *Neural computation*, 2006.
- [15] J. Schmidhuber, "Deep learning in neural networks: An overview," *arXiv preprint arXiv:1404.7828*, 2014.
- [16] A. Krizhevsky, I. Sutskever, and G. E. Hinton, "Imagenet classification with deep convolutional neural networks," in *Neural Information Processing Systems*, 2012.
- [17] D. Ciresan, U. Meier, and J. Schmidhuber, "Multi-column deep neural networks for image classification," in *IEEE Conference on Computer Vision and Pattern Recognition*, 2012.
- [18] M. Y. Shuiwang Ji, Wei Xu and K. Yu, "3d convolutional neural networks for human action recognition," in *International Conference on Machine Learning*. IEEE, 2010.
- [19] S. Ji, W. Xu, M. Yang, and K. Yu, "3d convolutional neural networks for human action recognition," *Pattern Analysis and Machine Intelligence, IEEE Transactions on*, 2013.
- [20] A. Mohamed, G. E. Dahl, and G. Hinton, "Acoustic modeling using deep belief networks," *Audio, Speech, and Language Processing, IEEE Transactions on*, 2012.
- [21] D. Wu and L. Shao, "Leveraging hierarchical parametric networks for skeletal joints based action segmentation and recognition," in *IEEE Conference on Computer Vision and Pattern Recognition*, 2014.
- [22] J. Ngiam, A. Khosla, M. Kim, J. Nam, H. Lee, and A. Y. Ng, "Multimodal deep learning," in *Proceedings of the 28th international conference on machine learning (ICML-11)*, 2011, pp. 689–696.
- [23] A. Hannun, C. Case, J. Casper, B. Catanzaro, G. Diamos, E. Elsen, R. Prenger, S. Satheesh, S. Sengupta, A. Coates *et al.*, "Deepspeech: Scaling up end-to-end speech recognition," *arXiv preprint arXiv:1412.5567*, 2014.
- [24] J. Shotton, A. Fitzgibbon, M. Cook, T. Sharp, M. Finocchio, R. Moore, A. Kipman, and A. Blake, "Real-time human pose recognition in parts from single depth images," in *IEEE Conference on Computer Vision and Pattern Recognition*, 2011.
- [25] J. Han, L. Shao, and J. Shotton, "Enhanced computer vision with microsoft kinect sensor: A review," *IEEE Transactions on Cybernetics*, vol. 43, no. 5, pp. 1317–1333, 2013.
- [26] "Multi-modal gesture recognition challenge 2013: Dataset and results." in *ACM ChaLearn Multi-Modal Gesture Recognition Grand Challenge and Workshop*, 2013. [Online]. Available: <http://gesture.chalearn.org/>
- [27] S. Fothergill, H. M. Mentis, P. Kohli, and S. Nowozin, "Instructing people for training gestural interactive systems," in *ACM Computer Human Interaction*, 2012.
- [28] I. Guyon, V. Athitsos, P. Jangyodsuk, B. Hamner, and H. J. Escalante, "Chalearn gesture challenge: Design and first results," in *IEEE Conference on Computer Vision and Pattern Recognition Workshops*, 2012.
- [29] J. Wang, Z. Liu, Y. Wu, and J. Yuan, "Mining actionlet ensemble for action recognition with depth cameras," in *IEEE Conference on Computer Vision and Pattern Recognition*, 2012.
- [30] M. Marszałek, I. Laptev, and C. Schmid, "Actions in context," in *IEEE Conference on Computer Vision & Pattern Recognition*, 2009.
- [31] H. Kuehne, H. Jhuang, E. Garrote, T. Poggio, and T. Serre, "HMDB: a large video database for human motion recognition," in *Proceedings of the International Conference on Computer Vision (ICCV)*, 2011.
- [32] S. Renals, N. Morgan, H. Bourlard, M. Cohen, and H. Franco, "Connectionist probability estimators in hmm speech recognition," *IEEE Transactions on Speech and Audio Processing*, vol. 2, no. 1, pp. 161–174, 1994.

- [33] H. Bourlard and N. Morgan, "Connectionist speech recognition-a hybrid approach," KLUWER ACADEMIC PUBLISHERS, Tech. Rep., 1994.
- [34] D. Wu and L. Shao, "Deep dynamic neural networks for gesture segmentation and recognition," *European Conference on Computer Vision and Pattern Recognition Workshops*, 2014.
- [35] L. Pigou, S. Dieleman, P.-J. Kindermans, and B. Schrauwen, "Sign language recognition using convolutional neural networks," in *European Conference on Computer Vision and Pattern Recognition Workshops*, 2014.
- [36] S. Nowozin and J. Shotton, "Action points: A representation for low-latency online human action recognition," Tech. Rep., 2012.
- [37] S. B. Wang, A. Quattoni, L.-P. Morency, D. Demirdjian, and T. Darrell, "Hidden conditional random fields for gesture recognition," in *Computer Vision and Pattern Recognition, 2006 IEEE Computer Society Conference on*, vol. 2. IEEE, 2006, pp. 1521–1527.
- [38] A. Dosovitskiy, J. T. Springenberg, M. A. Riedmiller, and T. Brox, "Discriminative unsupervised feature learning with convolutional neural networks," *CoRR*, 2014.
- [39] R. Socher, B. Huval, B. Bath, C. D. Manning, and A. Y. Ng, "Convolutional-recursive deep learning for 3d object classification," in *Advances in Neural Information Processing Systems*, 2012.
- [40] S. Gupta, R. Girshick, P. Arbeláez, and J. Malik, "Learning rich features from rgb-d images for object detection and segmentation," in *ECCV*. Springer, 2014.
- [41] "Chalearn looking at people challenge 2014: Dataset and results," in *European Conference on Computer Vision workshop*, 2014.
- [42] N. Neverova, C. Wolf, G. Taylor, and F. Nebout, "Multi-scale deep learning for gesture detection and localization," in *European Conference on Computer Vision and Pattern Recognition Workshops*, 2014.
- [43] C. Monnier, S. German, and A. Ost, "A multi-scale boosted detector for efficient and robust gesture recognition," in *European Conference on Computer Vision and Pattern Recognition Workshops*, 2014.
- [44] A. Yao, J. Gall, G. Fanelli, and L. J. Van Gool, "Does human action recognition benefit from pose estimation?," in *BMVC*, 2011.
- [45] X. Peng, L. Wang, and Z. Cai, "Action and gesture temporal spotting with super vector representation," in *European Conference on Computer Vision and Pattern Recognition Workshops*, 2014.
- [46] C. Bishop, *Pattern recognition and machine learning*. Springer, 2006.
- [47] A. Morris, A. Hagen, H. Glotin, and H. Bourlard, "Multi-stream adaptive evidence combination for noise robust asr," *Speech Communication*, 2001.
- [48] P.-J. Kindermans, H. Verschore, D. Verstraeten, and B. Schrauwen, "A P300 BCI for the masses: Prior information enables instant unsupervised spelling," in *Advances in Neural Information Processing Systems (NIPS)*, 2012, pp. 719–727.
- [49] R. Salakhutdinov, "Learning deep generative models," Ph.D. dissertation, University of Toronto, 2009.
- [50] R. Chaudhry, F. Ofli, G. Kurillo, R. Bajcsy, and R. Vidal, "Bio-inspired dynamic 3d discriminative skeletal features for human action recognition," in *IEEE Conference on Computer Vision and Pattern Recognition Workshops*, 2013.
- [51] M. Müller and T. Röder, "Motion templates for automatic classification and retrieval of motion capture data," in *SIGGRAPH/Eurographics symposium on Computer animation*. Eurographics Association, 2006.
- [52] F. Ofli, R. Chaudhry, G. Kurillo, R. Vidal, and R. Bajcsy, "Sequence of the most informative joints (smij): A new representation for human skeletal action recognition," *Journal of Visual Communication and Image Representation*, 2013.
- [53] V. Mnih, K. Kavukcuoglu, D. Silver, A. Graves, I. Antonoglou, D. Wierstra, and M. Riedmiller, "Playing atari with deep reinforcement learning," *arXiv preprint arXiv:1312.5602*, 2013.

- [54] K. Jarrett, K. Kavukcuoglu, M. Ranzato, and Y. LeCun, "What is the best multi-stage architecture for object recognition?" in *Computer Vision, 2009 IEEE 12th International Conference on*. IEEE, 2009, pp. 2146–2153.
- [55] G. E. Hinton, N. Srivastava, A. Krizhevsky, I. Sutskever, and R. R. Salakhutdinov, "Improving neural networks by preventing co-adaptation of feature detectors," *arXiv preprint arXiv:1207.0580*, 2012.
- [56] I. Sutskever, J. Martens, G. Dahl, and G. Hinton, "On the importance of initialization and momentum in deep learning," in *Proceedings of the 30th International Conference on Machine Learning (ICML-13)*, 2013, pp. 1139–1147.
- [57] N. Neverova, C. Wolf, G. W. Taylor, and F. Nebout, "Moddrop: adaptive multi-modal gesture recognition," *arXiv preprint arXiv:1501.00102*, 2014.
- [58] N. C. Camgöz, A. A. Kindiroglu, and L. Akarun, "Gesture recognition using template based random forest classifiers," in *Computer Vision-ECCV 2014 Workshops*. Springer, 2014, pp. 579–594.
- [59] J. Y. Chang, "Nonparametric gesture labeling from multi-modal data," in *European Conference on Computer Vision and Pattern Recognition Workshops*, 2014.
- [60] G. D. Evangelidis, G. Singh, and R. Horaud, "Continuous gesture recognition from articulated poses," in *Computer Vision-ECCV 2014 Workshops*. Springer, 2014, pp. 595–607.
- [61] G. Chen, D. Clarke, M. Giuliani, A. Gaschler, D. Wu, D. Weikersdorfer, and A. Knoll, "Multi-modality gesture detection and recognition with un-supervision, randomization and discrimination," in *Computer Vision-ECCV 2014 Workshops*. Springer, 2014, pp. 608–622.
- [62] B. Liang and L. Zheng, "Multi-modal gesture recognition using skeletal joints and motion trail model," in *Computer Vision-ECCV 2014 Workshops*. Springer, 2014, pp. 623–638.
- [63] F. Bastien, P. Lamblin, R. Pascanu, J. Bergstra, I. J. Goodfellow, A. Bergeron, N. Bouchard, and Y. Bengio, "Theano: new features and speed improvements," in *Deep Learning and Unsupervised Feature Learning NIPS 2012 Workshop*, 2012.
- [64] A. Graves, M. Liwicki, S. Fernández, R. Bertolami, H. Bunke, and J. Schmidhuber, "A novel connectionist system for unconstrained handwriting recognition," *Pattern Analysis and Machine Intelligence, IEEE Transactions on*, vol. 31, no. 5, pp. 855–868, 2009.
- [65] D. Wu and L. Shao, "Multimodal dynamic networks for gesture recognition," in *Proceedings of the ACM International Conference on Multimedia*. ACM, 2014, pp. 945–948.
- [66] K. Simonyan and A. Zisserman, "Very deep convolutional networks for large-scale image recognition," *arXiv preprint arXiv:1409.1556*, 2014.

Di Wu Biography text here.

Lionel Pigou Biography text here.

1
2
3 **Pieter-Jan Kindermans** Biography text here.
4
5
6
7
8
9
10
11
12
13
14
15 **Nam Le** Biography text here.
16
17
18
19
20
21
22
23
24
25
26
27
28 **Ling Shao** Biography text here.
29
30
31
32
33
34
35
36
37
38
39
40 **Joni Dambre** Biography text here.
41
42
43
44
45
46
47
48
49
50
51
52 **Jean-Marc Odobez** Biography text here.
53
54
55
56
57
58
59
60

Deep Dynamic Neural Networks for Multimodal Gesture Segmentation and Recognition

Di Wu, Lionel Pigou, Pieter-Jan Kindermans, Nam Le, Ling Shao, Joni Dambre, and Jean-Marc Odobez

Abstract—This paper describes a novel method called deep dynamic neural networks (*DDNN*) for multimodal gesture recognition. More precisely, a semi-supervised hierarchical dynamic framework based on a Hidden Markov Model (HMM) is proposed for simultaneous gesture segmentation and recognition where skeleton joint information, depth and RGB images are the multimodal input observations. Unlike most traditional approaches which rely on the construction of complex handcrafted features as HMM input features, our approach learns high-level spatio-temporal representations using deep neural networks suited to the input modality: a Gaussian-Bernoulli deep belief networks (*DBN*) to handle skeletal dynamics, and a 3D convolutional neural networks (*3DCNN*) to manage and fuse batches of depth and RGB images. This achieved through the modeling and learning of the emission probabilities of the HMM required to infer the gesture sequence. This purely data driven approach achieves a score of **0.81** in the ChaLearn LAP gesture spotting challenge. The performance is on par with a variety of the state-of-the-art hand-tuned feature based approaches and other learning based methods. Thus opening the door for using deep learning techniques to further explore multimodal time series.

Index Terms—Deep learning, convolutional neural networks, deep belief networks, hidden Markov models, gesture recognition.

1 INTRODUCTION

In recent years, human action recognition has drawn increasing attention of researchers, primarily due to its potential in areas such as video surveillance, robotics, human-computer interaction, user interface design, and multimedia video retrieval.

Previous works on video-based motion recognition [1], [2], [3] mainly focused on adapting handcrafted features. These methods usually have two stages: an optional feature detection stage followed by a feature description stage. Well-known feature detection methods (“interest point detectors”) are Harris3D [4], Cuboids [5] and Hessian3D [6]. For descriptors, popular methods are Cuboids [7], HOG/HOF [4], HOG3D [8] and Extended SURF [6]. In recent work of Wang *et al.* [9], dense trajectories with improved motion based descriptors epitomised the pinnacle of handcrafted features and achieved state-of-the-art results on a variety of “in the wild” datasets. Based on the current trends, challenges and interests within the action recognition community, it is to be expected that many successes will follow. However, the very high-dimensional and dense trajectory features usually require the use of advanced dimensionality reduction methods to make them computationally feasible.

Furthermore, as discussed in the evaluation paper of Wang *et al.* [10], no universally best hand-engineered feature exists and the best performing feature descriptor is often dataset dependent. This clearly indicates that the ability to learn dataset specific feature extractors can be highly beneficial. For this reason, even though handcrafted features have dominated image recognition in previous years, there has been a growing interest in learning low-level and mid-level features, either in supervised, unsupervised, or semi-supervised settings [11], [12], [13].

Since the recent resurgence of neural networks invoked

by Hinton and others [14], deep neural architectures serve as an effective solution for extracting high-level features from data. Deep artificial neural networks have won numerous contests in pattern recognition and representation learning. Schmidhuber [15] compiled a historical survey compactly summarising relevant works with more than 850 entries of credited works. From this overview we see that these models have been successfully applied to a plethora of different domains: the GPU-based cuda-convnet [16] classifies 1.2 million high-resolution images into 1000 different classes; multi-column deep neural networks [17] achieve near-human performance on the handwritten digits and traffic signs recognition benchmarks; 3D convolutional neural networks [18] [19] recognise human actions in surveillance videos; deep belief networks combined with hidden Markov models [20] [21] for acoustic and skeletal joints modelling outperform the decade-dominating paradigm of Gaussian mixture models in conjunction with hidden Markov models. Multimodal deep learning technique were also investigated [22] to learn cross-modality representation, for instance in the context of audio-visual speech recognition. And recently, Baidu research proposed a DeepSpeech system [23] that combines a well-optimised recurrent neural network (RNN) training system, achieving the best error rate on noisy speech dataset. In these fields, deep architectures have shown great capacity to discover and extract higher level relevant features.

However, direct and unconstrained learning of complex problems remains difficult, since (i) the amount of required training data increases steeply with the complexity of the prediction model and (ii) training highly complex models with very general learning algorithms is extremely difficult. It is therefore a common practice to restrain the complexity of the model. This is generally done by operating on small patches to reduce the input dimension and diversity [13], or by training the model in an unsupervised manner [12], or

1 by forcing the model parameters to be identical for different
 2 input locations (as in convolutional neural networks [16],
 3 [17], [18]).

4 On the sensor side, due to the immense popularity of
 5 Microsoft Kinect [24] [25], there has been a recent interest in
 6 developing methods for human gesture and action recogni-
 7 tion from 3D skeletal data and depth images. A number of
 8 new datasets [26], [27], [28], [29] have provided researchers
 9 with the opportunity to design novel representations and
 10 algorithms, and test them on a much larger number of
 11 sequences. While gesture recognition based on 3D joint
 12 positions may seem trivial, it is actually not the case due
 13 to several factors. A first one is the high dimensionality
 14 and the large amount of variability of the pose space itself.
 15 A second aspect that further complicates the recognition is
 16 the segmentation of the different gestures. While in practice
 17 segmentation is as important as the recognition, it is an
 18 often neglected aspect of the current action recognition
 19 research which often assume the availability of segmented
 20 inputs [4] [30] [31].

21 In this paper we aim to address these issues by propos-
 22 ing a data driven system, focusing on analysis of acyclic
 23 video sequence labelling problems, *i.e.* video sequences that
 24 are non-repetitive as opposed to longer repetitive activities,
 25 *e.g.* jogging, walking and running. By integrating deep
 26 neural networks within an HMM temporal framework, our
 27 work allows the online joint recognition and segmentation
 28 of gestures. This framework is inspired by discriminant H-
 29 MM, which embedded multi-layer perceptron inside HMM,
 30 in continuous speech recognition [32] [33]. This paper is
 31 an extension of the works of [21], [34] and [35]. The key
 32 contributions can be summarised as follows:

- 33 • A Gaussian-Bernoulli Deep Belief Network is proposed
 34 to extract high-level skeletal joint features and the
 35 learned representation is used to estimate the emission
 36 probability needed to infer gesture sequences;
- 37 • A 3D Convolutional Neural Network is proposed to
 38 extract features from 2D multiple channel inputs like
 39 depth and RGB images stacked along the 1D temporal
 40 domain;
- 41 • Intermediate and late fusion strategies are investigat-
 42 ed within the temporal modelling. The result of both
 43 mechanisms show that multiple-channel fusions out-
 44 perform individual modules.

45 The remainder of this paper is organised as follows.
 46 Section II reviews related works for gesture recognition with
 47 various temporal models and recent deep learning work on
 48 RGB-D data. Section III introduces the formulation of our
 49 Deep Dynamic Neural Network model and the intuition
 50 behind the high level feature extraction. Section IV details
 51 the model implementation. Section V details the experimen-
 52 tal analysis and Section VI concludes the paper with
 53 discussions related to future works.

54 2 RELATED WORK

55 Gesture recognition has drawn increasing attention of re-
 56 searchers, primarily due to its growing potential in areas
 57 such as robotics, human-computer interaction and user
 58 interface design. Different temporal models have been pro-
 59 posed. Nowozin and Shotton [36] proposed the notion of

60 “action points” to serve as natural temporal anchors of sim-
 61 ple human actions using a Hidden Markov Model. Wang *et*
 62 *al.* [37] introduced a more elaborated discriminative hidden-
 63 state approach for the recognition of human gestures. How-
 64 ever, relying on only one layer of hidden states, their model
 65 alone might not be powerful enough to learn a higher level
 66 representation of the data and take advantage of very large
 67 corpus. In this paper, we adopt a different approach by
 68 focusing on deep feature learning within a temporal model.

69 There have been a few works exploring deep learning
 70 for action recognition in videos. For instance, Ji *et al.* [19]
 71 proposed using 3D convolutional neural network for auto-
 72 mated recognition of human actions in surveillance videos.
 73 Their model extracts features from both the spatial and
 74 the temporal dimensions by performing 3D convolutions,
 75 thereby capturing the motion information encoded in mul-
 76 tiple adjacent frames. To further boost the performance, they
 77 proposed regularising the outputs with high-level features
 78 and combining the predictions of a variety of different
 79 models. Taylor *et al.* [11] also explored 3D convolutional
 80 networks for learning spatio-temporal features for videos.
 81 The experiments in [34] show that multiple network aver-
 82 aging works better than a single individual network and
 83 larger nets will generally perform better than smaller nets.
 84 Providing there is enough data, averaging multi-column
 85 nets [17] applied to action recognition could also further
 86 improve the performance.

87 However, the advent of Kinect-like sensors has put more
 88 emphasis on RGB-D data for gesture recognition, but not
 89 only. For instance, the benefits of deep learning using RGB-
 90 D data have been explored for object detection or classifi-
 91 cation tasks. Dosovitskiy *et al.* [38] presented a generic feature
 92 learning for training a convolutional network using only
 93 unlabeled data. In contrast to supervised network training,
 94 the resulting feature representation is not class specific and
 95 are advantageous on geometric matching problems, outper-
 96 forming the SIFT descriptor. Socher *et al.* [39] proposed a
 97 single convolutional neural net layer for each modality as
 98 inputs to multiple, fixed-tree RNNs in order to compose
 99 higher order features for 3D object classification. The single
 100 convolutional neural net layer provides useful translational
 101 invariance of low level features such as edges and allows
 102 parts of an object to be deformable to some extent. To ad-
 103 dress object detection, Gupta *et al.* [40] proposed a geocentric
 104 embedding for depth images that encodes height above
 105 ground and angle with gravity for each pixel in addition
 106 to the horizontal disparity. This augmented representation
 107 allows CNN to learn stronger features than when using
 108 disparity (or depth) alone.

109 Recently, the gesture recognition domain itself has been
 110 stimulated by the collection of large public corpus. In par-
 111 ticular, the ChaLearn LAP [41] gesture spotting challenge
 112 has collected around 14,000 gestures drawn from a vocab-
 113 uary of 20 Italian sign gesture categories. The emphasis
 114 is on multi-modal automatic learning gestures performed
 115 by several different users, with the aim of performing user
 116 independent continuous gesture spotting. Some of the top
 117 winning methods in the ChaLearn LAP gesture spotting
 118 challenge require a set of complicated handcrafted features
 119 for either skeletal input, RGB-D input, or both. For instance,
 120 Neveroa *et al.* [42] proposed a pose descriptor consisting

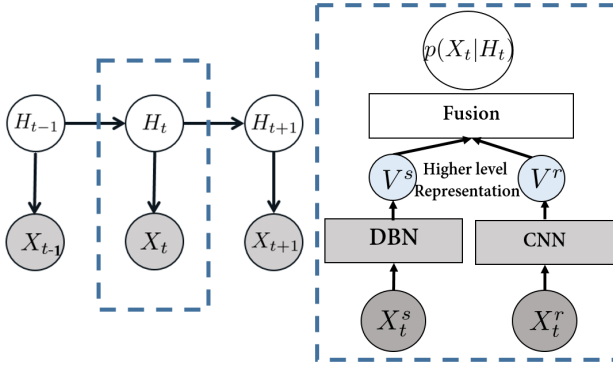


Fig. 1: Gesture recognition model: the temporal model is a HMM (left), whose emission probability $p(X_t|H_t)$ (right) is modeled by forward-linked neural networks. More precisely, observations X_t (skeletal features X_t^s , or RGB-D image features X_t^r) are first passed through appropriate deep neural nets (a Deep Belief Network -DBN- pretrained with Gaussian-Bernouilli Restricted Boltzmann Machines for the skeleton modality, and a 3D convolutional neural network -3DCNN- for the RGB-D modality) to implicitly extract high-level features (V^s and V^r) which are further fused to produce an estimate of $p(X_t|H_t)$.

of 7 logical subsets for skeleton features while Monnier *et al.* [43] proposed to use 4 types of features for skeleton features (normalised joint positions; joint quaternion angles; Euclidean distances between specific joints; and directed distances between pairs of joints, based on the features proposed by Yao *et al.* [44]) and histograms of oriented gradients (HOG) descriptor for RGB-D images around hand regions. In [45], the state-of-the-art dense trajectory [9] hand-crafted features are adopted for the RGB module.

There is a gradual trend to learn the features for gesture recognition in videos. For instance, the recent methods in [34], [35] focused on single modalities, used deep networks to learn representations from skeleton data [34] or from RGB-D data [35]. Neverova *et al.* [42] presents a multi-scale and multimodal deep network for gesture detection and localisation. Key to their technique is a training strategy that exploits i) careful initialisation of individual modalities and ii) gradual fusion of modalities from the strongest to weakest cross-modality structure. One major difference compared to what we propose is the treatment of the time factor: rather than using a temporal model, they used frames within a fixed interval as the input of their neural networks for the prediction of the final gesture class, an approach that requires to train several multi-scale temporal networks to cope with gestures performed at different speeds. Furthermore, their skeleton features used in their network are sets of ad-hoc hand crafted features, rather than being learned from raw data.

3 MODEL FORMULATION & OVERALL APPROACH

Inspired by the framework successfully applied to speech recognition [20], the proposed model is a data driven learning system. This results in an integrated model, where the amount of prior knowledge and engineering is minimised. On top of that, this approach works without the need for additional complicated preprocessing and dimensionality

reduction methods as it is naturally embedded in the framework.

The proposed approach relies on a Hidden Markov Model (HMM) for the temporal part, and neural networks to model the emission probabilities. In the remainder of this section, we will first present our temporal model and then introduce its main component. The details of the two distinct neural networks and fusion mechanisms along with post-processing will be provided in Section 4.

3.1 Deep Dynamic Neural Networks

The proposed deep dynamic neural network (DDNN) can be seen as an extension of [21], where instead of only using the restricted Boltzmann machines to model human motion, various connectivity layers (fully connected layers, convolutional layers) are stacked together to learn higher level features justified by a variational bound [14] from different input modules.

A continuous-observation HMM is adopted for modelling higher level temporal relationships. At each time step t , we have one observed random variable X_t composed of the skeleton input X_t^s and RGB-D input images X_t^r as shown in the graphical representation in Fig. 1. The hidden state variable H_t takes on values in a finite set \mathcal{H} composed of $N_{\mathcal{H}}$ states related to the different gestures. The intuition motivating the HMM model is that a gesture is composed of a sequence of poses where the relative duration of each pose may vary. This variance is captured by allowing flexible forward transitions within a Markov chain. In practice, H_t can be interpreted as being in a particular phase of a gesture a .

Classically under the HMM assumption, the joint probability of observations and states is given by:

$$p(H_{1:T}, X_{1:T}) = p(H_1)p(X_1|H_1) \prod_{t=2}^T p(X_t|H_t)p(H_t|H_{t-1}), \quad (1)$$

where $p(H_1)$ is the prior on the first hidden state, $p(H_t|H_{t-1})$ is the transition dynamics modelling the allowed state transitions and their probabilities, and $p(X_t|H_t)$ is the emission probability of the observation, modelled by deep neural networks in our case. These elements are presented below.

3.2 State-transition model and inference

The HMM framework can be used for simultaneous gesture segmentation and recognition. This is achieved by defining the state transition diagram as shown in Fig 2. For each given gesture $a \in \mathcal{A}$, a set of states \mathcal{H}_a is introduced to define a Markov model of that gesture. For example, for action sequence “tennis serving”, the action sequence can implicitly be dissected into $h_{a_1}, h_{a_2}, h_{a_3}$ as: 1) raising one arm 2) raising the racket 3) hitting the ball. More precisely, since our goal is to capture the variation in speed of the performed gestures, we set the transition matrix $p(H_t|H_{t-1})$ in the following way: when being in a particular node n at time t , moving to time $t+1$, we can either stay in the same node (slower), move to node $n+1$, or move to node $n+2$ (faster). Furthermore, to allow the segmentation of gestures, we add an ergodic state (\mathcal{E}) which resembles

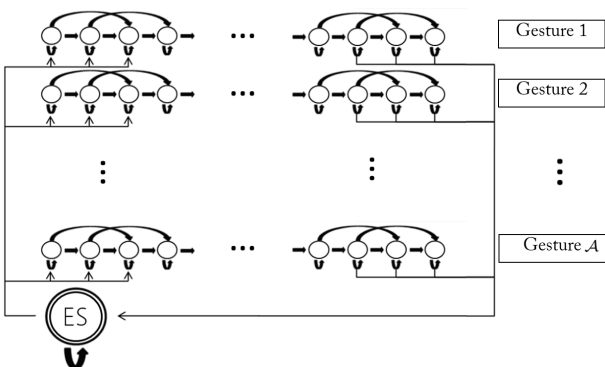


Fig. 2: State diagram of the *ES-HMM* model for low-latency gesture segmentation and recognition. An ergodic state (\mathcal{ES}) is used to model the resting position between gesture sequences. Each node represents a single state and each row represents a single gesture model. The arrows indicate possible transitions between states.

the silence state for speech recognition and which serve as a catch-all state. From this state we can move to the first three nodes of any gesture class, and from the last three nodes of any gesture class we can move to \mathcal{ES} . Hence, the hidden variable H_t can take values within the finite set $\mathcal{H} = (\bigcup_{a \in \mathcal{A}} \mathcal{H}_a) \cup \{\mathcal{ES}\}$.

Overall, we refer to the model as the ergodic states hidden Markov model (*ES-HMM*) for simultaneously gesture segmentation and recognition. It differs from the firing hidden Markov model of [36] in that we strictly follow a left-right HMM structure without allowing backward transition, forbidding inter-states transverse, assuming that the considered gestures do not undergo cyclic repetitions as in walking for instance.

Once we have the trained model, we can use standard techniques to infer online the filtering distribution $p(H_t|X_{1:t})$, or offline (or with delay) the smoothed distribution $p(H_t|X_{1:T})$ where T denotes the end of the sequence. Because the graph for the hidden Markov model is a directed tree, this problem can be solved exactly and efficiently using the max-sum algorithm also known as Viterbi algorithm. This algorithm searches the space of paths efficiently to find the most probable path with a computational cost that grows only linearly with the length of the chain [46]. The result of the Viterbi algorithm is a path-sequence $\hat{h}_{t:T}$ of nodes going through the state diagram of Fig. 2 and from which we can easily infer the class of the gesture as illustrated in Fig. 8.

3.3 Learning the emission probability

Traditionally, emission probabilities for activity recognition have been trained with Gaussian Mixture Models (GMM), one per state. Alternatively, in this work we propose to model this term in a discriminative fashion. More precisely, since the input features have a high dimensionality, we propose to learn them using two distinctive types of neural networks suited to the input modality, as summarized in the right of Fig. 1.

Unfortunately, estimating a probability density such as an emission probability remains quite a difficult problem,

especially in high dimensions. Theoretically, discriminative neural networks estimate posterior probabilities $p(H_t|X_t)$. We should divide posteriors by priors to get the scaled likelihoods which are required by the HMM for decoding. However, using scaled likelihood may not be beneficial if estimated priors do not match the priors in the test set [47]. Therefore, we employ the posteriors directly without dividing by the priors. This is equivalent to assuming that all priors are equal. or, in other words, inference in the HMM only depends only on the ratio between emission probabilities for the different states. One can interpret that the models are trained to directly predict the ratio between emission probabilities. This is similar to the approach used by Kindermans et al. to integrate transfer learning and an HMM based language model into a single probabilistic model [48]. One should think of the predicted emission probability ratio as an unnormalized version of the true emission probability. Nevertheless, to simplify the discussion of our models for readers with a basic understanding of HMMs, we will refer to the predicted emission probability ratio simply as emission probabilities since the underlying model remains unchanged.

For the skeletal features, we rely on a Deep-Belief Network (DBN) trained in two steps [49]: in the first step, stacked Restricted Boltzmann Machines (RBM) is trained in an unsupervised fashion using only observation data to learn high-level feature representations; in the second step, the model is used as a Deep-Belief Network whose weights are further fine-tuned for learning the emission probability. For the RGB and depth (RGB-D) video data, we rely on a 3D (2D for space and 1D for time) convolutional neural networks (3DCNN) to model the emission probabilities. Finally, a fusion method combines in an intermediate or in a late stage the contributions of both modalities. In all cases (including the fusion), the supervised training is conducted by learning to predict the state label (an element of \mathcal{H}) associated to each training or testing frame.

Such an approach present several advantages over the traditional GMM paradigm. First, while GMMs are easy to fit when they have diagonal covariance matrices and, with enough components, can model any distribution, they have been shown to statistically inefficient at modeling high-dimensional features with many componential structure as explained in [20]. For instance, assume that the components of the input feature space can be separated into two subspaces characterized by N and M significantly different patterns in the training data, respectively, and that the occurrences of these patterns are relatively independent¹. A GMM will require $N * M$ components to model this structure because each component must generate all the input features. On the other hand, a stacked RBMs model that can explain the data using multiple causes only requires $N + M$ components (in the ideal fully independent case), each of which is specific to a particular subspace. This exponential inefficiency of GMMs at modeling factorial structures leads to GMM+HMM systems having a very large number of Gaussians, most of which must be estimated from a very small fraction of the data.

1. In our case, intuitively these spaces could be the features from different body parts, like left/right arm or torso features.

Secondly, the approach for training the skeleton DBN model, first using variational learning to train stacked RBMs with unlabeled data, then in a discriminative fashion [49] has been shown to have several advantages. It has been observed that variational learning [14], which tries to optimize the data-likelihood while minimizing the Kullback-Leibler divergence between the true posterior distribution of the hidden state (i.e. hidden layer variables of the RBMs in our case) and an approximation of this distribution, tends to produce unimodal distributions. This is beneficial, as this means that similar sensory inputs will be mapped to similar hidden variables. Thus, the intuition for using DBN for modeling the emission probability $p(X_t|H_t)$ from skeleton joints is that by learning the multi-layer network layer by layer, semantically meaningful high level features for skeleton configuration will be extracted while at the same time a parametric prior of human pose is learned. In our case, using the pair wise joints features as raw input, the data-driven approach network will be able to extract relational multi-joints features which are relevant to the target classes. For instance, from the “toss” action data, a wrist joints rotating around shoulder joints feature is expected to be extracted from the backpropagation learning, and be the equivalent of those task specific *ad hoc* hard wired sets of joints configurations defined in [50] [51] [36] [52].

The benefit of such a learning approach is even more important when large amount of unlabelled data (e.g. skeleton data inferred from depth images of people performing unknown gestures) is available in addition to the labeled ones (this was not the case in this paper). Naturally, many of the features learned in this unsupervised way might be irrelevant for making the required discriminations, even though they are important for explaining the input data. However, this is a price worth paying if data availability and computation are cheap and lead to a stable mapping of the high-dimensional input into high-level features that are very good for discriminating between classes of interest. In this view, it is important to notice that each weight in a neural network is usually constrained by a larger fraction of the training samples than each parameter in a GMM, a point that has been masked by other differences in training. In particular, neural networks have traditionally been training discriminatively, whereas GMMs are typically trained as generative models, which given their parametric nature partially compensate the fact that each mixture of a large GMM is usually trained on a very small fraction of the data.

In summary, the feed forward neural networks offer several potential advantages over GMMs:

- their estimation of emission probabilities does not require detailed assumptions about the data distribution;
- they allow an easy combination of diverse features, including both discrete and continuous features;
- they use far more of the data to constrain each parameter because the output on each training case is sensitive to a large fraction of the weights.

4 MODEL IMPLEMENTATION

In this section, we detail the different component of the proposed Deep Dynamic Neural Network approach.

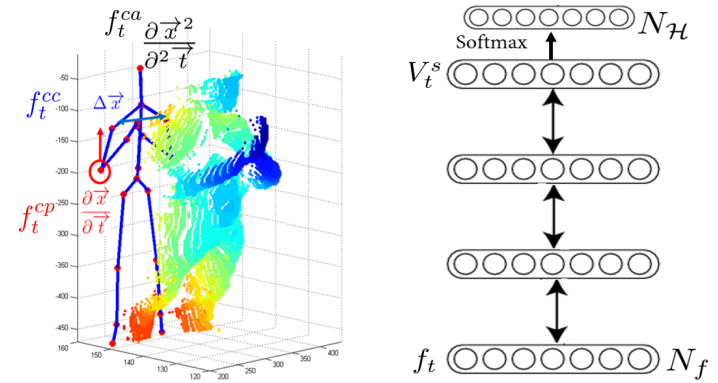


Fig. 3: Left: A point cloud projection of a depth image and the 3D positional features. Right: A DBN is trained to predict the emission probability $p(X_t^s|H_t)$ from the skeleton input f_t . The double arrows indicate that the intermediate weights are first trained in an unsupervised fashion using stacked RBMs.

4.1 Ergodic States Hidden Markov Model

In all our experiments, the different modelling elements are specified as follows.

The number of states N_{H_a} associated to an individual gesture has been set to 5. Therefore, in total, the number of states is $N_H = 20 \times 5 + 1 = 101$ when conducting experiments on the Chalearn dataset containing 20 classes. Note that intuitively, 5 states represents a good granularity as most gestures in the Chalearn are composed of 5 phases: an onset, followed by arm motions to reach a more static pose (often characterized by a distinct hand posture), and the motion back to the rest place. In the future, optimal section of this number² and of different number of states per gesture could be investigated.

The training data in Chalearn is given as a set of sequences $\mathbf{x}_i = [x_{i,1}, \dots, x_{i,t}, \dots, x_{i,T_i}]$ where $x_{i,t} = [x_{i,t}^s, x_{i,t}^r]$ corresponds to the skeleton and RGB-D input. As only a single gesture label is provided for each sequence, we need to define $\mathbf{y}_i = [y_{i,1}, \dots, y_{i,t}, \dots, y_{i,T_i}]$, the sequence of state labels $y_{i,t}$ associated to each frame. To do so, a force alignment is used which means that if the i^{th} sequence is a gesture a , then the first $\lfloor \frac{T_i}{5} \rfloor$ frames are assigned to state h_a^1 (the first state of gesture a), the following $\lfloor \frac{T_i}{5} \rfloor$ frames are assigned to h_a^2 , and so forth.

Note that each gesture sequence comes with the video frames preceding and following the gesture. In practice, we extracted 5 frames before and after each gesture sequence and labelled them with the ergodic state (\mathcal{ES}) label. The transitional matrix $p(H_t|H_{t-1})$ was learned by simply collecting the transition statistics from the label sequences \mathbf{y}_i , allowing 5 frame jumps to accommodate skipping states.

4.2 Skeleton Module

4.2.1 Skeleton input features

Given our task, only the $N_j = 11$ upper body joints are relevant and considered, namely “ElbowLeft, WristLeft, ShoulderLeft, HandLeft, ElbowRight, WristRight, ShoulderRight, HandRight, Head, Spine, HipCenter”. The raw skeleton features of time t are defined as $x_t^s = [x_t^{s,1}, \dots, x_t^{s,N_j}]$. To

²Experiments with 10 states led to similar performance.

capture the gesture dynamics, rather than using x_t^s as raw input to our data driven approach, we follow the approach of [21] and compute the 3D positional pairwise differences of joints as well as temporal derivatives, defined as (as shown in Fig. 3) ³:

$$f_t^{cc} = \{x_t^{s,i} - x_t^{s,j} | i, j = 1, 2, \dots, N_j; i \neq j\} \quad (2)$$

$$f_t^{cp} = \{x_{t+1}^{s,i} - x_t^{s,i} | i = 1, 2, \dots, N_j\} \quad (3)$$

$$f_t^{ca} = \{x_{t+1}^{s,i} - 2 \times x_t^{s,i} + x_{t-1}^{s,i} | i = 1, 2, \dots, N_j\} \quad (4)$$

This results in an input feature vector $\mathbf{f}_t = [f_t^{cc}, f_t^{cp}, f_t^{ca}]$ of dimension $N_f = N_j \times (\frac{N_j}{2} + N_j + N_j) * 3 = 891$. Admittedly, here we do not completely neglect human prior knowledge about information extraction for relevant static postures, velocity and acceleration of overall dynamics of motion data. While we have indeed used prior knowledge to define our relevant features, we believe they remain quite general and do not need dataset specific tuning. Note that the feature extraction process resembles the computation of the *Mel Frequency Cepstral Coefficients (MFCCs)* and their temporal derivatives typically used in the speech recognition community [20].

4.2.2 Modeling X_t^s using Deep Belief Networks

Given the input skeleton feature \mathbf{f} , a *DBN* model is used to predict the emission probability, as shown in Fig. 3. As explained in Section 3.3, the learning proceeds in two steps: in the first one, the network is considered as a stack of RBMs, and trained using a greedy, layer-by-layer unsupervised learning algorithm [14]; in the second one, a softmax network layer is added on top of the RBMs to create a *DBN* architecture, where the weights of the first step are used to initialize the corresponding weights in the *DBN*, and the *DBN* is further trained and fine-tuned in a supervised fashion to predict the emission probability. The number of nodes at each layer of the *DBN* are $[N_f, 2000, 2000, 1000, N_H]$. We provide below further details on the model and training.

Gaussian-Bernoulli RBM. Restricted Boltzmann machine (RBM) are undirected graphical models involving visible and hidden variables, with symmetric connections between the hidden and visible units but no connection within hidden variables or visible variables. In most cases, RBMs rely on binary random variables. However, in our case the visible unit in the first layer are the vector of skeleton features $\mathbf{f} \in \mathbf{R}^{N_f}$, which are continuous. To account for this situation, we thus resort to a Gaussian-Bernoulli RBM (GRBM) [49], whose main difference w.r.t. standard RBM lies in the following: the energy term of our first layer \mathbf{f} to the hidden binary stochastic units $\mathbf{h} \in \{0, 1\}^F$ is given by:

$$E(\mathbf{f}, \mathbf{h}; \theta) = - \sum_i \frac{(f_i - b_i)^2}{2\sigma_i^2} - \sum_i \sum_j W_{ij} h_j \frac{f_i}{\sigma_i} - \sum_j a_j h_j \quad (5)$$

where $\theta = \{W, b, a\}$ are the free parameters: $W_{i,j}$ serves as the symmetric synergy term between visible unit i and hidden unit j , while b_i and a_j are the bias term of the visible

3. Note that the offset features used in [21] depend on the first frame. Thus if the initialisation fails which is a very common scenario, the feature descriptor will be generally very noisy. Hence, here we do not use these offset features.

and hidden units, respectively. The conditional distributions needed for inference and generation are given by the traditional logistic function g for the binary hidden variable, and the normal distribution \mathcal{N} for the continuous variable:

$$P(h_j = 1 | \mathbf{f}) = g(\sum_i W_{ij} f_i + a_j) \quad (6)$$

$$P(f_i = f | \mathbf{h}) = \mathcal{N}(f | \mu_i, \sigma_i^2). \quad (7)$$

where $\mu_i = b_i + \sigma_i^2 \sum_j W_{ij}$. In practice, we normalise the data (mean subtraction and standard deviation division) in the preprocessing phase. Hence, instead of learning σ_i^2 , one typically used $\sigma_i^2 = 1$ during training.

We ran 100 epochs using a fixed recipe based on stochastic gradient descent with a mini-batch size of 200 training cases to train the stacked RBM, in which the learning rate is fixed at 0.001 for the Gaussian-Bernoulli RBMs, and at 0.01 for the following binary-binary RBMs.

DBN forward training. The *DBN* is initialized with the result of the previous step, a method which tends to avoid suboptimal local minima and increase the networks performance stability. The learning rate for the parameter fine tuning starts at 1 with 0.99999 mini-batch scaling. During the experiments, early stopping occurs around epoch 440. The optimisation completes with a frame based validation error rate of 16.5%.

4.3 RGB & Depth 3D Module

4.3.1 Preprocessing

Although DeepMind technology [53] presented the first deep learning model to successfully learn control policies directly from high-dimensional sensory input using deep reinforcement learning, working directly with raw input Kinect recorded data frames, which are 640×480 pixel images, can be computationally demanding. Therefore, our first step in the preprocessing stage consists of cropping the highest hand and the upper body using the given joint information. In the ChaLearn dataset, we determined that the highest hand is the most interesting. When both hands are used, they normally perform the same (mirrored) movement, and when one hand is used, it is always the highest one which is relevant. Furthermore, to be invariant to handedness, we always train the model with the right hand view. That is, when the left hand is actually the performing hand, the video was mirrored.

The preprocessing results in four video samples (body and hand with grayscale and depth) of resolution 64×64 . Furthermore, the noise in the depth maps is reduced by removing the background using the automatically produced segmentation mask provided with the data, and applying a median filtering. Depth images are Z-normalised (the mean is subtracted -as it is rather irrelevant to the gesture subclass- and the result divided by the standard deviation), whereas RGB images are only normalized by the image standard deviation. The outcome is illustrated in Fig. 5.

4.3.2 3DCNN Architecture

This architecture consists of a series of layers composed of either convolution, pooling or, in the last layer, fully connected layers. The 3D convolution itself is achieved by

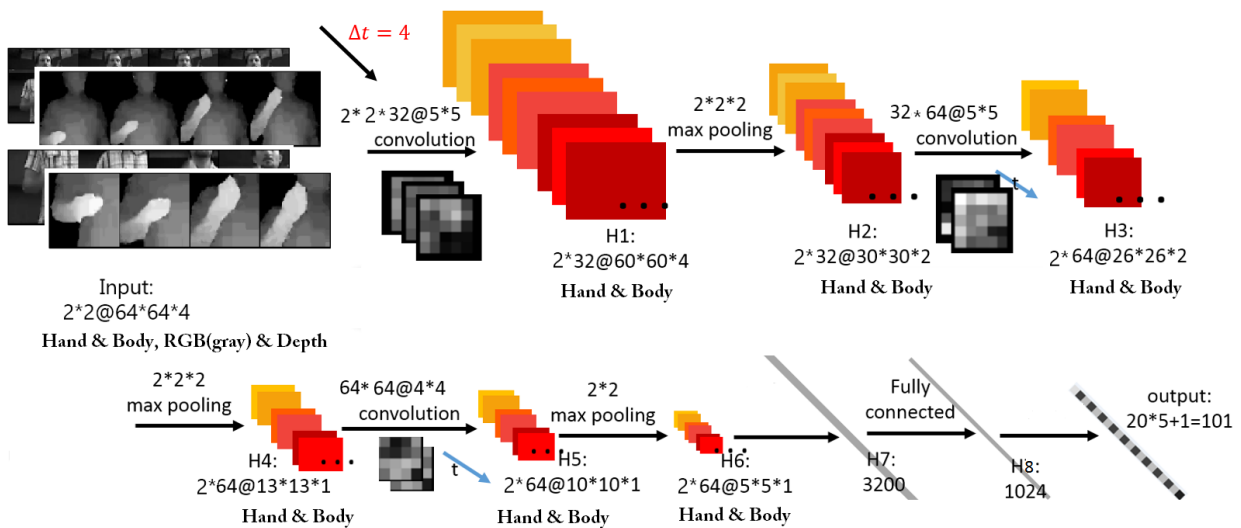


Fig. 4: 3DCNN architecture. The input is $2 \times 2 @ 64 \times 64 \times 4$, meaning 2 modalities (depth and RGB) for the hand and body regions, each being 4 consecutive 64 by 64 frames stacked together. See text for further details.

convolving a 3D kernel to the cuboid formed by stacking multiple contiguous frames together. We follow the nomenclature of in [19]. However, instead of using *tanh* units [19], Rectified Linear Units (*ReLUs*) [16] were used in order to speed up training. Formally, the value of a unit at position (x, y, z) (z here corresponds to the time-axis) in the j -th feature map in the i -th layer, denoted as v_{ij}^{xyz} , is given by:

$$v_{ij}^{xyz} = \max(0, (b_{ij} + \sum_m \sum_{p=0}^{P_i-1} \sum_{q=0}^{Q_i-1} \sum_{r=0}^{R_i-1} w_{ijm}^{pqr} v_{(i-1)m}^{(x+p)(y+q)(t+r)})) \quad (8)$$

The complete 3DCNN architecture is depicted in Fig. 4: 4 types of input contextual frames are stacked as size $64 \times 64 \times 4$ (as illustrated in Fig. 5). The first layer (H1) consists of 32 feature maps produced by 5×5 spatial convolutional kernels, followed by local contrast normalisation (LCN) [54]. Note that the filter response maps of the Depth and RGB images of the hand (and body) are summed to produce a single feature map, thus resulting in H1 in 32 feature maps for each of the hand and for the body region. A 3D max pooling with strides $(2, 2, 2)$ is then applied. The second layer uses 64 feature maps with 5×5 kernels followed by LCN and 3D max pooling with strides $(2, 2, 2)$. The third layer is composed of 64 feature maps with 4×4 kernels followed by 3D max pooling with strides $(1, 2, 2)$. All hand and body convolutional layer outputs of H6 are flattened in H7, and fed into one fully connected layer of size 1024. Finally, the output layer has N_H values, the number of states in the HMM state diagram (see Fig. 2).

4.3.3 Details of Learning

During training, dropout [55] is used as main regularisation approach to reduce overfitting. Nesterovs accelerated gradient descent (NAG) [56] with a fixed momentum-coefficient of 0.9 and mini-batches of size 64 are also used. The learning rate is initialised at 0.003 with a 5% decrease after each epoch. The weights of the 3DCNNs are randomly initialised with a normal distribution with $\mu = 0$ and $\sigma = 0.04$. The frame based validation error rate is 39.06% after 40

epochs. Compared with the skeleton module (16.5% validation error rate), the 3DCNN has a notable higher frame based error rate.

4.3.4 Looking into the Networks: visualisation of Filter Banks

The convolutional filter weights of the first layer are depicted in Fig. 5. The unique characteristics from the kernels are clearly visible: as hand input images (RGB and depth) have larger homogenous areas than the body inputs, the resulting filters are smoother than their body counterpart. In addition, while being smoother overall than the grayscale filters, depth filters exhibit stronger edges, as also reported in [39]. Finally, by looking at the joint depth-image response maps, we can notice that some filters better capture segmentation like information, while other are more edge oriented.

4.4 Multimodal Fusion

To combine the two modalities, two strategies can be used, as shown in Fig. 6: a late fusion approach and an intermediate fusion approach.

4.4.1 Late Fusion

This scheme fuses the combination of the emission probabilities estimated from the different input. While different combinatin schemes exist, here we considered a simple linear combination:

$$\log p(X_t | H_t) \propto \alpha \cdot \log p(X_t^s | H_t) + (1 - \alpha) \cdot \log p(X_t^r | H_t) \quad (9)$$

where the different emission probabilities are provided by the modules described in 4.2 and 4.3, and α is a coefficient that controls the contributions of each source of information and which is estimated by cross validation. Interestingly, the best performing α is close to 0.5, indicating that both modalities are equally important.

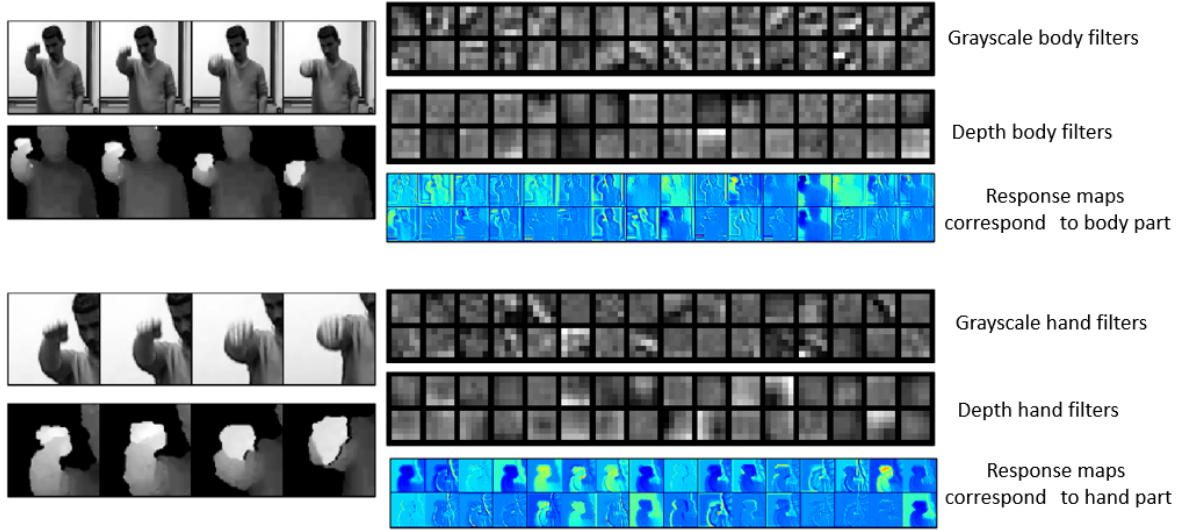


Fig. 5: Visualisation of input frames, first convolutional layer 5×5 filters, and corresponding response maps. As depth images are smoother than the grayscale ones, the corresponding filter are smoother as well.

4.4.2 Intermediate Fusion

As an alternative to the late fusion scheme, we can take advantage of the high-level representation implicitly learned by each module (and represented by the V^s and V^r nodes of the penultimate layer of the respective networks, before the softmax) to fuse the modality in an intermediate fashion by concatenating these two layers in one layer of 2024 hidden unites and learning a cross-modality emission probability predictive network. Note that this is very similar in spirit to the approach proposed in [22] for audio-visual speech recognition. An important difference is that in [22], the same stacked RBMs/DBN architecture was used to represent both modalities before fusion, whereas in our case, a stacked RBMs/DBN and a 3DCNN are used. Also, [22] proposed the use of a multimodal autoencoder to handle predictions when potentially only one modality might be present, a point that we do not address.

The resulting architecture is trained by first initializing the weights of the deeper layers from the previously trained module, and then jointly fine tuning the whole network (including learning the last layer parameters) and stop the training when the validation error rate stops decreasing (~ 15 epochs). We argue that using the “pre-trained” parameters is important due to the heterogeneity of the inputs of the system, and that the joint training should adjust parameters to handle this heterogeneity and produce the final estimates.

5 EXPERIMENTS AND ANALYSIS

This Section reports the experiments performed to validate our model. First, we will introduce the ChaLearn dataset, and then present the experimental protocol we followed. In Section 5.3, we will present and analyse the obtained results, including a discussion on the modeling elements. Finally, Section 5.4 will briefly discuss the computational complexity of the approach.

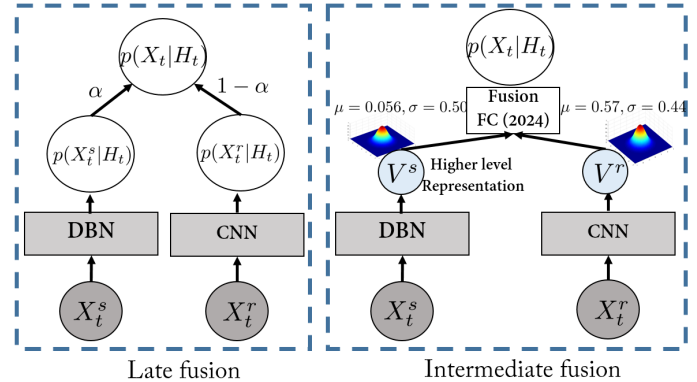


Fig. 6: Multimodal dynamic networks with late fusion scheme (left) and intermediate fusion scheme (right). The late approach simply combines the emission probabilities from two modalities. In the intermediate fusion scheme, each modality (skeleton and RGB-D) is first pre-trained separately, and their high-level representation V^s and V^r (the penultimate node layers of their neural networks) are concatenated to generate a shared representation. The resulting architecture is trained jointly.

5.1 Chalearn LAP Dataset

The dataset used in this work is provided by the ChaLearn LAP [41] gesture spotting challenge⁴. The focus is on “multiple instance, user independent spotting” of gestures, which means learning to recognize gestures from several instances for each category performed by different users, drawn from a gesture vocabulary of 20 Italian cultural/anthropological signs. A gesture vocabulary is a set of unique gestures, generally related to a particular task.

The challenge dataset contains 940 video sequences, each performed by a single person and composed of 10 to 20 gesture instances for a total of around 14,000 gestures. There are 20 gesture classes, i.e. *vattene*, *vieniqui*, *perfetto*,

4. <http://gesture.chalearn.org/2014-looking-at-people-challenge/data-2014-challenge>



Fig. 7: Examples of gestures in the ChaLearn dataset. This dataset is challenging because the “user independent” setting (a)&(b), some of gestures differ primarily in hand pose but not the overall arm motions (d)&(e) and some gestures require both hands to perform (g,h,i). Subtle hand movement (c) and differences in performing speed and range (f) also make recognising tasks challenging.

furbo, cheduepalle, chevuoi, daccordo, seipazzo, combinato, fre-ganiente, ok, cosatifarei, basta, prendere, noncenepiu, fame, tan-totempo, buonissimo, messidaccordo, sonostufo, with a number a samples well balanced between classes. The average length of gestures is 39 frames, the minimum frame number for a gesture is 16 and the maximum frame number is 104.

This dataset is challenging because the “user independent” setting and some of gestures differ primarily in hand pose but not the overall arm motions as illustrated in Fig. 7. In terms of data, three modalities are provided with the input videos: the sequence of skeleton joints, and the RGB and depth images (including a segmentation of the person performing the gesture).

5.2 Experimental protocol

5.2.1 Training and evaluation protocol

We follow the ChaLearn experimental protocol, in which the input sequences are split into 700 videos for training, and 240 sequences for testing and reporting results. Note that the test sequences are not segmented a priori and the gestures must be detected within a continuous data stream which, in addition to the targeted gestures, also contains noisy and out-of-vocabulary gestures. Furthermore, in the experiments, we split the training videos into 650 videos for learning the actual neural network model parameters, and 50 videos used as validation data for monitoring the training performance or selecting hyper-parameters.

5.2.2 Performance measures

Several measures can be used to evaluate the gesture recognition performance. In this work, we adopted the ChaLearn

Module	Validation	Test
Skeleton – DBDN	0.783	0.779
RGB-D – 3DCNN	0.752	0.717
Multimodal Late Fusion	0.817	0.809
Multimodal Inter. Fusion	0.800	0.798

TABLE 1: Results in terms of Jaccard index JI for the different network structures and modalities modeling the emission probabilities.

performance measure known as the Jaccard index, which relies on a frame-by-frame prediction accuracy. More precisely, if GT_i denotes the sequence of ground truth labels in video i , and R_i the algorithm output, the Jaccard index of the video is defined as:

$$JI_i(GT_i, R_i, g) = \frac{N_s(GT_i, R_i, g)}{N_u(GT_i, R_i, g)}, \quad (10)$$

$$\text{and } JI_i = \frac{1}{|\mathcal{G}_i|} \sum_{g \in \mathcal{G}_i} JI_i(GT_i, R_i, g) \quad (11)$$

where $N_s(GT_i, R_i, g)$ denotes the number of frames where the ground truth and result agree on the gesture class g , and $N_u(GT_i, R_i, g)$ denotes the number of frames labeled as a gesture frame g by either the ground truth or the algorithm, and \mathcal{G}_i denotes the set of gestures either in the ground truth or detected by the algorithm in sequence i^5 . The average of the JI_i over all test videos is reported as performance measure. Note that experimentally, this measure tends to favours having more false positives than missing true positives, in order to increase the numerator.

Being defined at the frame level, the Jaccard index can vary due to variations of the segmentation (both in the ground truth and recognition) at gesture boundaries, which can be irrelevant from an application viewpoint. Thus, we also defined performance at the gesture event level by following the commonly used PASCAL challenge intersection over union criterion. More precisely, if for a gesture segment G , we have $\frac{|G \cap R|}{|G \cup R|} > 0.5$, where R denotes a recognized gesture segment of the same class, then the gesture is said to be recognized. If the same relation holds but with a gesture segment of another class, the prediction is incorrect. Otherwise the gesture is rated as undetected. This allows us to define the *Recognized*, *Confused* and *Missed* performance measures at the video level, which are further averaged over test sequences for reporting.

5.2.3 Tested systems

We evaluated the recognition performance made by the HMM applied to the emission probabilities estimated from either the skeleton data, the RGB-D image data, the late fusion scheme, and the intermediate fusion scheme. Note that in all cases the HMM output was further filtered to avoid false alarms, by considering gesture segments of less than 20 frames as noise and discarding them.

5.3 Results

Overall results. The overall performance of the algorithms are given in Tables 1 and 2. As can be observed from both performance measures, the skeleton module usually

5. Note that ‘non gesture’ frames are thus excluded from the counts.

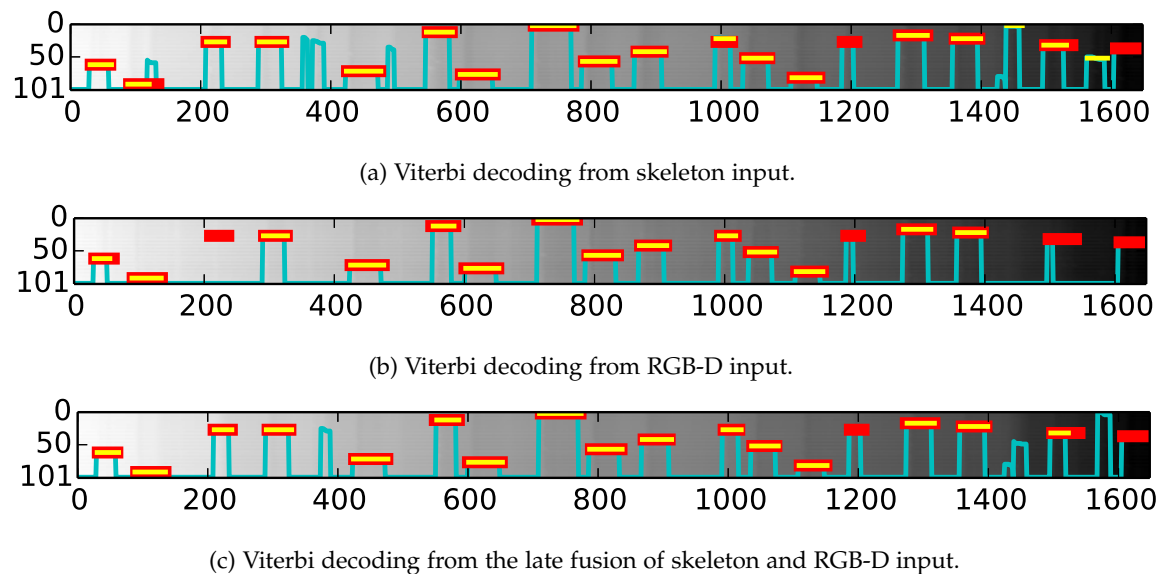


Fig. 8: Viterbi decoding of sample sequence #700, using skeleton (top), RGB-D (middle) and late fusion system (bottom). The x-axis represents time and the y-axis represents the hidden states of all classes and of the ergodic state (state 101). The cyan lines represent the viterbi shortest path, while red lines denote the ground truth labels, and the yellow segments are the predicted labels. The fusion method exploits the complementary properties of individual modules, e.g. around frame 200 the skeleton help solving the missed detection from the 3DCNN module, while around frame 1450, the 3DCNN module can help suppress the false positive prediction made by the skeleton module.

performs better than the RGB-D module. In addition, its generalization capability is better than that of the RGB-D module, especially when measured with the Jaccard index where there is almost no drop of performance between the validation and test data. One possible explanation is that the information in the skeleton data is more robust, as it benefited from training using huge and highly varied data [24]: around one million images from both realistic and synthetic depth images were used to train the decision forest classifiers involved in the joints extraction. On the other hand, as the RGB-D module relies on the raw data and was learned only from the ChaLearn training set, it may suffer from some overfitting. Another interesting conclusion that can be drawn from Table 2 is that while most errors from the RGB-D module are due to under detection (the *Missed* rate is 19.7%, whereas it is only 4.1% for the skeleton), the skeleton module is more reactive to gesture activity, but makes more mistakes (the *Confused* rate is 12.3% vs 4.5% for RGB-D).

Finally, the results also demonstrate that the combination of both modalities is more robust, as shown by the recognition rate increase and the smaller drop in the generalization performance (for instance the decrease of the *Recognized* rate is lower than for the skeleton data alone).

Confusion matrices. The confusion matrices (in log-form) in Fig. 9 better illustrate the complementarity of the behaviors of the two modalities. The higher underdetection of RGB-D is clearly visible (whiter matrix, except last 'undetected' column). We can also notice that some gestures are more easily recognized than others, or catch the difficult instances of other gestures. This is the case of the "Basta" gesture, whose arms motion resembles the start and end of the arm motion of many other gesture (see Fig. 7). Whatever the modality, its model thus tends to recognize few instances of all other gesture classes, whenever their likelihood are

	%	Validation	Test
Skeleton - DBDN	<i>Recognized</i>	86.3	83.6
	<i>Confused</i>	11.4	12.3
	<i>Missed</i>	2.3	4.1
RGB-D - 3DCNN	<i>Recognized</i>	78.7	75.8
	<i>Confused</i>	5.2	4.5
	<i>Missed</i>	16.1	19.7
Multimodal Late Fusion	<i>Recognized</i>	87.9	86.4
	<i>Confused</i>	9.1	8.7
	<i>Missed</i>	3.0	4.9
Multimodal Inter. Fusion	<i>Recognized</i>	86.5	85.5
	<i>Confused</i>	7.3	6.8
	<i>Missed</i>	6.2	7.7

TABLE 2: Gesture classification performance at the event level, in percentage of the number of ground truth gestures.

low when being evaluated using the HMM states associated with their true label due to too much variability. Similarly, the hand movement and pose of the "Buenissimo" gesture is present in several other gesture classes, whose instances are then often confused with "Buenissimo" when relying on the skeleton information alone. However, as these gestures differ primarily in their hand pose, such confusion is much more reduced using the RGB-D domain, or when fusing the skeleton and RGB-D modules. The complementary properties of the two modalities is also illustrated from the Viterbi path decoding plot in Fig. 8. In general, the benefit of this complementarity between arm pose/gesture and hand pose can be observed from the whiter confusion matrix than in the skeleton case (less confusion due to hand pose information from RGB-D) and much less under-detection than in the RGB-D case (better upper-body pose discrimination thanks to skeleton input).

However, the modalities by themselves have more difficulties to correct the recognition errors which are due to variations coming from the performer, like differentiating

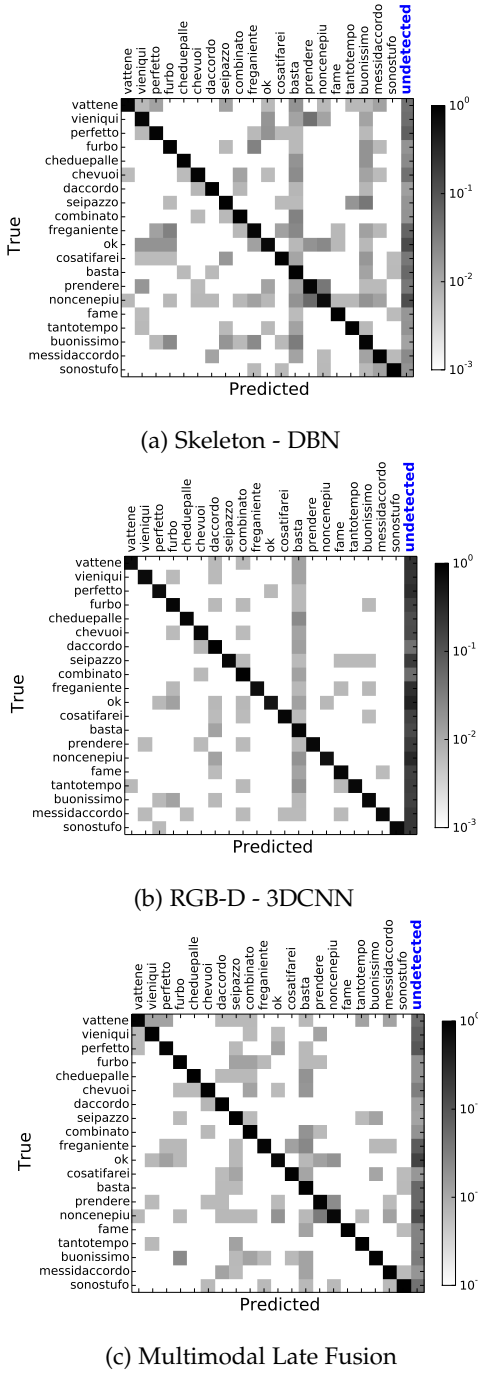


Fig. 9: Confusion Matrices (log-norm) for the different modalities.

people that gesticulate more (see Fig. 11).

Late vs. Intermediate fusion. The results in Tab. 1 and 2 show that the intermediate fusion system improved individual modalities, but without outperforming the late fusion system. The result is counter-intuitive, as we would have expected the cross-modality learning in the intermediate fusion scheme to result in better emission probability predictions, as compared to the simple score fusion in the late system. One possible explanation is that the independence assumption of the late scheme better preserves both the complementarity and redundancy of the different modalities,

properties which are important for fusion. Another related explanation is that in the intermediate fusion learning process, one modality may dominate and skew the network towards learning that specific module and lowering the importance of the other one. The large difference between the mean activations of the skeleton module neurons which are predominantly larger than those of the RGB-D ConvNet's (0.57 vs. 0.056) can be an indicator of such a bias during the multimodal fine-tuning phase and support this conjecture, even if these mean activations are not directly comparable due to the neuron heterogeneity (the skeleton DBN has logistic units whereas the 3DCNN ConvNet has relu units). Note that such heterogeneity was not present when fusing modalities in [22], where better registration and less spatial registration variability in lip images allowed to also resort to the same stacked RBMs for the visual modality (rather than 3DCNN) and the audio one. More investigation on how to handle heterogeneous networks should be conducted.

HMM benefit. As the emission probabilities are learned in a discriminative manner, one could wonder whether the HMM brings benefit beyond smoothing. To investigate this issue, we removed the temporal structure as follows: for a given gesture a , we computed its score at time t , $\text{Score}(a, t)$, by summing the emission probabilities $p(X_t | H_t = h)$ for all nodes associated to that gesture, i.e. $h \in \mathcal{H}_a$. This score is then smoothed in the temporal domain (using a window of 5 frames) to obtain $\bar{\text{Score}}(a, t)$. Finally, following [57], the gesture recognition proceeds in two steps: first finding gesture segments by thresholding the score of the ergodic state; then, for each resulting gesture segment, the recognized gesture is defined as the one whose average score within the segment is the highest. Fig. 10 illustrates this process along with the DDNN and ground-truth. In general, we could observe that better decisions on the presence of gestures and on the boundaries where a gesture starts and ends are achieved with the proposed DDNN thanks to the use of the state-diagram defined in Fig. 2, as compared to the above method, where deciding on a gesture detection threshold is rather unstable and quite sequence dependent. Indeed, the overall performance of the above scheme without the HMM temporal sequencing is reduced to $J_1 = 0.66$, while the *Recognized*, *Confused* and *Missed* corresponding to Table 2 for the test set are 76.6, 5.3 and 18.1. However, note that the above method relying on only the gesture probability learned using neural networks on 5 frame inputs still outperforms the Jaccard index of 0.413 obtained by [58] when using a 5 frames template matching system where all the features are handcrafted.

Comparison with the state-of-the-art. The performance of recent state-of-the-art techniques is given in Table 3. The first half of the table resort to hand crafted feature approaches and then usually a second stage classifier. Our proposed system performs on par with the top two methods. However, hand crafted feature methods' performance are saturated regardless of the increase training data. The representation learning methods in the second half of the Table perform comparably with the best hand crafted feature approaches and the top representation method achieves the best Jaccard index score. Given more training data, it is expected that the networks will be able to be more adapted to the "user in-

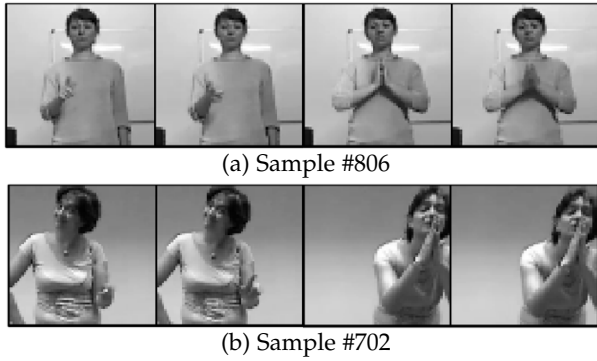


Fig. 11: Examples of performer variations in the upper body dynamic. Most performers tend to keep their upper-body static while performing the gesture, leading to good recognition performance (Jaccard index of person on the top is 0.95 for the late fusion system). Some persons are more involved and move more vehemently (person at the bottom, Jaccard index of 0.61), which can affect the recognition algorithm itself (bottom left samples) or even the skeleton tracking (bottom right; note that normally cropped images are centered vertically on the head position).

Module	Skeleton	RGB-D	Fusion
[43] 3 set skeletal & HOG, Boosted classifier	0.791	-	0.822
[59] 3D skeletal pose & HOG, MRF	0.790	-	0.827
[45] Dense trajectory (HOG, HOF, MBH)	-	0.792	-
[58] Template based Random Forest Classifier	-	-	0.747
[60] Fisher Vector, Dynamic Programming	0.745	-	-
[61] Independent Subspace Analysis, RF	-	0.649	-
[62] PHOG, SVM, HMM	0.454	0.462	0.597
[42] Representation Learning (multiscal)	0.808	0.809	0.849
[35] CNN	-	0.789	-
[34] Deep Neural Networks	0.747	0.637	0.804
DDNN (this work)	0.779	0.717	0.809

TABLE 3: Comparison of results in terms of the ChaLearn Jaccard index with state-of-the-art related works.

dependent” setting. It also worths noting that our proposed system is the only method that incorporates the temporal modelling element rather than sliding window approach. We believe this is an interesting research direction that can be more adapted to various lengths of gestures and relevant temporal factors.

5.4 Computational Complexity

We can distinguish between two complexities: the training one, and the test one.

Complexity at training time. Although training deep neural network using stochastic gradient descent is computationally intensive, the reuse of pre-trained network parameters as done in our case can help with better initialisation and lead to faster convergence. We can observe different training time in function of the modality (and architecture). Specifically, using a modern GPU (GeForce GTX TITAN Black) and conv op. by Theano [63], the training time of each epoch of the DBN skeleton module is less than 300 seconds and allows training the required 500 epochs within 2 days. The training time of each epoch of the 3DCNN RGB-D module is much more expensive, taking more than 10,000 seconds. Hence, 40 epochs takes around 5 days to train. The

fusion network being initialised with the individual module parameters, its training time is half that of the 3DCNN.

Complexity at test time. Given the learned models, our framework with the above GPU can perform real-time video sequence labelling with a low inference cost. More specifically, a single feed forward neural network incurs linear computational time ($\mathcal{O}(T)$), and is efficient because it requires only matrix products and convolution operations. The complexity of the Viterbi algorithm is itself of $\mathcal{O}(T * |S|^2)$, where T is the number of frames and $|S|$ the number of states, and thus performs real-time given our state-space. In practice, our multimodal neural network can be deployed at 90 FPS. The preprocessing part takes most of the time and our un-optimized version runs at 25 FPS, while the Viterbi decoding runs at 90 FPS. Hence, the overall system can achieve faster than real-time performance.

6 CONCLUSION AND FUTURE WORK

Hand-engineered, task-specific features are often task-specific and time-consuming to design. This difficulty is even more pronounced with multimodal data as we would like the features to relate to multiple data sources. In this paper, we presented a novel deep dynamic neural network (DDNN) for learning contextual frame-level representations and modelling emission probabilities in the framework of an HMM temporal model. Different feature learning methods (DBN and 3DCNN) suited to the heterogeneous inputs from skeletal joints, RGB images, and depth images were proposed, as well as different fusion schemes. Experimental results on bi-modal gesture time series show that the multimodal DDNN framework can learn good models of the joint space of multiple sensory inputs, improving over unimodal input.

There are several directions for future work. Our results with those of other recent works suggest that learning features directly from data is a very important research direction and that with more and more data and flops-free computational power, learning-based methods are not only more generalisable to many domains, but also are powerful in combination with other well-studied probabilistic graphical models for dynamical modelling and reasoning. In this view, the learning of better shared and complementary representation among multimodal and heterogeneous inputs, as done in [57], requires more exploration. In addition, while the proposed HMM provided a good basis for the temporal modeling of gestures, other more discriminant temporal approaches such as Conditional Random Field or further and better variants [37] could be directly exploited at their advantage in conjunction with our deep neural network learning approach. Ultimately, in a logical way, these two research directions converge into the investigation of a single and unified deep learning framework fusing heterogeneous modalities by using recent Recurrent Neural Networks such as Long Short Term Memory [64] for modelling the temporal component of the problem.

APPENDIX A

DETAILS OF THE CODE

The python code using Theano [63] for this work can be found at:

https://github.com/stevenwudi/chalearn2014_wudi_l1o

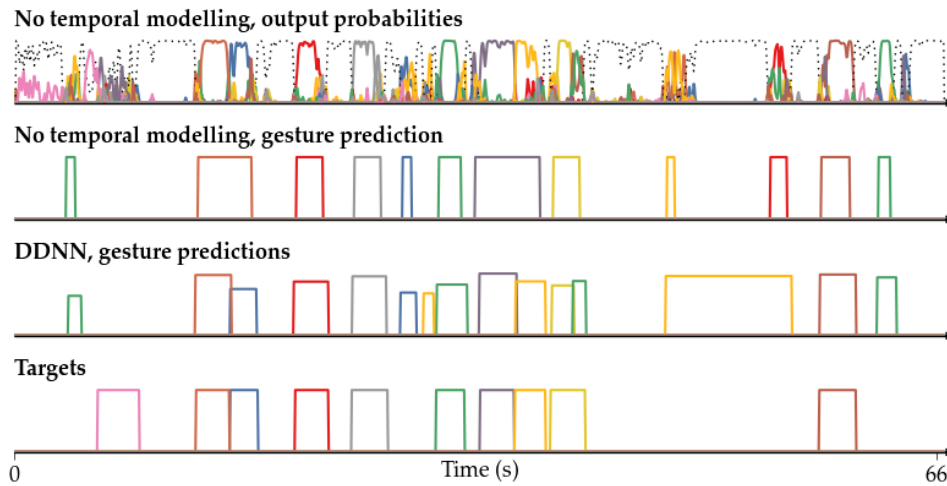


Fig. 10: HMM temporal contribution. First row: output emission probabilities for each gesture as given by the late fusion scheme (see text) for the test set #703. The dashed line represents the probability of the Resting/Other gesture state, while other colour represent different gestures. Second row: resulting recognized gestures, without HMM modeling. Third row: HMM output. Fourth row: ground truth segmentation. Without temporal modelling, the decision boundary of a gesture will be more rugged and it is more difficult to make hard decisions of where the gesture starts or ends. Hence, in general, it causes miss-detection and miss-merging. Thanks to the HMM temporal modelling and Viterbi path decoding, gesture boundaries are usually cleaner defined from the Resting state to the gesture states, resembling the behavior of the manual annotators with better accuracy.

REFERENCES

- [1] L. Liu, L. Shao, F. Zheng, and X. Li, "Realistic action recognition via sparsely-constructed gaussian processes," *Pattern Recognition*, doi: 10.1016/j.patcog.2014.07.006., 2014.
- [2] L. Shao, X. Zhen, and X. Li, "Spatio-temporal laplacian pyramid coding for action recognition," *IEEE Transactions on Cybernetics*, vol. 44, no. 6, pp. 817-827, 2014.
- [3] D. Wu and L. Shao, "Silhouette analysis-based action recognition via exploiting human poses," *IEEE Transactions on Circuits and Systems for Video Technology*, vol. 23, no. 2, pp. 236-243, 2013.
- [4] I. Laptev, "On space-time interest points," *International Journal of Computer Vision*, 2005.
- [5] P. Dollár, V. Rabaud, G. Cottrell, and S. Belongie, "Behavior recognition via sparse spatio-temporal features," in *Visual Surveillance and Performance Evaluation of Tracking and Surveillance*. IEEE, 2005.
- [6] G. Willems, T. Tuytelaars, and L. V. Gool, "An efficient dense and scale-invariant spatio-temporal interest point detector," in *European Conference on Computer Vision*. Springer, 2008.
- [7] P. Scovanner, S. Ali, and M. Shah, "A 3-dimensional sift descriptor and its application to action recognition," in *International Conference on Multimedia*. ACM, 2007.
- [8] A. Klaser, M. Marszalek, and C. Schmid, "A Spatio-Temporal Descriptor Based on 3D-Gradients," in *British Machine Vision Conference*, 2008.
- [9] H. Wang, A. Kläser, C. Schmid, and C.-L. Liu, "Dense trajectories and motion boundary descriptors for action recognition," *International Journal of Computer Vision*, 2013.
- [10] H. Wang, M. M. Ullah, A. Klaser, I. Laptev, C. Schmid *et al.*, "Evaluation of local spatio-temporal features for action recognition," in *British Machine Vision Conference*, 2009.
- [11] G. W. Taylor, R. Fergus, Y. LeCun, and C. Bregler, "Convolutional learning of spatio-temporal features," in *European Conference on Computer Vision*. Springer, 2010.
- [12] Q. V. Le, W. Y. Zou, S. Y. Yeung, and A. Y. Ng, "Learning hierarchical invariant spatio-temporal features for action recognition with independent subspace analysis," in *IEEE Conference on Computer Vision and Pattern Recognition*, 2011.
- [13] M. Baccouche, F. Mamalet, C. Wolf, C. Garcia, and A. Baskurt, "Spatio-temporal convolutional sparse auto-encoder for sequence classification," in *British Machine Vision Conference*, 2012.
- [14] G. E. Hinton, S. Osindero, and Y.-W. Teh, "A fast learning algorithm for deep belief nets," *Neural computation*, 2006.
- [15] J. Schmidhuber, "Deep learning in neural networks: An overview," *arXiv preprint arXiv:1404.7828*, 2014.
- [16] A. Krizhevsky, I. Sutskever, and G. E. Hinton, "Imagenet classification with deep convolutional neural networks," in *Neural Information Processing Systems*, 2012.
- [17] D. Ciresan, U. Meier, and J. Schmidhuber, "Multi-column deep neural networks for image classification," in *IEEE Conference on Computer Vision and Pattern Recognition*, 2012.
- [18] M. Y. Shuiwang Ji, Wei Xu and K. Yu, "3d convolutional neural networks for human action recognition," in *International Conference on Machine Learning*. IEEE, 2010.
- [19] S. Ji, W. Xu, M. Yang, and K. Yu, "3d convolutional neural networks for human action recognition," *Pattern Analysis and Machine Intelligence, IEEE Transactions on*, 2013.
- [20] A. Mohamed, G. E. Dahl, and G. Hinton, "Acoustic modeling using deep belief networks," *Audio, Speech, and Language Processing, IEEE Transactions on*, 2012.
- [21] D. Wu and L. Shao, "Leveraging hierarchical parametric networks for skeletal joints based action segmentation and recognition," in *IEEE Conference on Computer Vision and Pattern Recognition*, 2014.
- [22] J. Ngiam, A. Khosla, M. Kim, J. Nam, H. Lee, and A. Y. Ng, "Multimodal deep learning," in *Proceedings of the 28th international conference on machine learning (ICML-11)*, 2011, pp. 689-696.
- [23] A. Hannun, C. Case, J. Casper, B. Catanzaro, G. Diamos, E. Elsen, R. Prenger, S. Satheesh, S. Sengupta, A. Coates *et al.*, "Deepspeech: Scaling up end-to-end speech recognition," *arXiv preprint arXiv:1412.5567*, 2014.
- [24] J. Shotton, A. Fitzgibbon, M. Cook, T. Sharp, M. Finocchio, R. Moore, A. Kipman, and A. Blake, "Real-time human pose recognition in parts from single depth images," in *IEEE Conference on Computer Vision and Pattern Recognition*, 2011.
- [25] J. Han, L. Shao, and J. Shotton, "Enhanced computer vision with microsoft kinect sensor: A review," *IEEE Transactions on Cybernetics*, vol. 43, no. 5, pp. 1317-1333, 2013.
- [26] "Multi-modal gesture recognition challenge 2013: Dataset and results," in *ACM ChalLearn Multi-Modal Gesture Recognition Grand Challenge and Workshop*, 2013. [Online]. Available: <http://gesture.challearn.org/>
- [27] S. Fothergill, H. M. Mentis, P. Kohli, and S. Nowozin, "Instructing people for training gestural interactive systems," in *ACM Computer Human Interaction*, 2012.
- [28] I. Guyon, V. Athitsos, P. Jangyodsuk, B. Hamner, and H. J. Escalante, "ChalLearn gesture challenge: Design and first results," in *IEEE Conference on Computer Vision and Pattern Recognition Workshops*, 2012.
- [29] J. Wang, Z. Liu, Y. Wu, and J. Yuan, "Mining actionlet ensemble

- for action recognition with depth cameras," in *IEEE Conference on Computer Vision and Pattern Recognition*, 2012.
- [30] M. Marszałek, I. Laptev, and C. Schmid, "Actions in context," in *IEEE Conference on Computer Vision & Pattern Recognition*, 2009.
- [31] H. Kuehne, H. Jhuang, E. Garrote, T. Poggio, and T. Serre, "HMDB: a large video database for human motion recognition," in *Proceedings of the International Conference on Computer Vision (ICCV)*, 2011.
- [32] S. Renals, N. Morgan, H. Bourlard, M. Cohen, and H. Franco, "Connectionist probability estimators in hmm speech recognition," *IEEE Transactions on Speech and Audio Processing*, vol. 2, no. 1, pp. 161–174, 1994.
- [33] H. Bourlard and N. Morgan, "Connectionist speech recognition—a hybrid approach," KLUWER ACADEMIC PUBLISHERS, Tech. Rep., 1994.
- [34] D. Wu and L. Shao, "Deep dynamic neural networks for gesture segmentation and recognition," *European Conference on Computer Vision and Pattern Recognition Workshops*, 2014.
- [35] L. Pigou, S. Dieleman, P.-J. Kindermans, and B. Schrauwen, "Sign language recognition using convolutional neural networks," in *European Conference on Computer Vision and Pattern Recognition Workshops*, 2014.
- [36] S. Nowozin and J. Shotton, "Action points: A representation for low-latency online human action recognition," Tech. Rep., 2012.
- [37] S. B. Wang, A. Quattoni, L.-P. Morency, D. Demirdjian, and T. Darrell, "Hidden conditional random fields for gesture recognition," in *Computer Vision and Pattern Recognition, 2006 IEEE Computer Society Conference on*, vol. 2. IEEE, 2006, pp. 1521–1527.
- [38] A. Dosovitskiy, J. T. Springenberg, M. A. Riedmiller, and T. Brox, "Discriminative unsupervised feature learning with convolutional neural networks," *CoRR*, 2014.
- [39] R. Socher, B. Huval, B. Bath, C. D. Manning, and A. Y. Ng, "Convolutional-recursive deep learning for 3d object classification," in *Advances in Neural Information Processing Systems*, 2012.
- [40] S. Gupta, R. Girshick, P. Arbeláez, and J. Malik, "Learning rich features from rgbd images for object detection and segmentation," in *ECCV*. Springer, 2014.
- [41] "Chalearn looking at people challenge 2014: Dataset and results," in *European Conference on Computer Vision workshop*, 2014.
- [42] N. Neverova, C. Wolf, G. Taylor, and F. Nebout, "Multi-scale deep learning for gesture detection and localization," in *European Conference on Computer Vision and Pattern Recognition Workshops*, 2014.
- [43] C. Monnier, S. German, and A. Ost, "A multi-scale boosted detector for efficient and robust gesture recognition," in *European Conference on Computer Vision and Pattern Recognition Workshops*, 2014.
- [44] A. Yao, J. Gall, G. Fanelli, and L. J. Van Gool, "Does human action recognition benefit from pose estimation?," in *BMVC*, 2011.
- [45] X. Peng, L. Wang, and Z. Cai, "Action and gesture temporal spotting with super vector representation," in *European Conference on Computer Vision and Pattern Recognition Workshops*, 2014.
- [46] C. Bishop, *Pattern recognition and machine learning*. Springer, 2006.
- [47] A. Morris, A. Hagen, H. Glotin, and H. Bourlard, "Multi-stream adaptive evidence combination for noise robust ast," *Speech Communication*, 2001.
- [48] P.-J. Kindermans, H. Verschore, D. Verstraeten, and B. Schrauwen, "A P300 BCI for the masses: Prior information enables instant unsupervised spelling," in *Advances in Neural Information Processing Systems (NIPS)*, 2012, pp. 719–727.
- [49] R. Salakhutdinov, "Learning deep generative models," Ph.D. dissertation, University of Toronto, 2009.
- [50] R. Chaudhry, F. Ofli, G. Kurillo, R. Bajcsy, and R. Vidal, "Bio-inspired dynamic 3d discriminative skeletal features for human action recognition," in *IEEE Conference on Computer Vision and Pattern Recognition Workshops*, 2013.
- [51] M. Müller and T. Röder, "Motion templates for automatic classification and retrieval of motion capture data," in *SIGGRAPH/Eurographics symposium on Computer animation*. Eurographics Association, 2006.
- [52] F. Ofli, R. Chaudhry, G. Kurillo, R. Vidal, and R. Bajcsy, "Sequence of the most informative joints (smij): A new representation for human skeletal action recognition," *Journal of Visual Communication and Image Representation*, 2013.
- [53] V. Mnih, K. Kavukcuoglu, D. Silver, A. Graves, I. Antonoglou, D. Wierstra, and M. Riedmiller, "Playing atari with deep reinforcement learning," *arXiv preprint arXiv:1312.5602*, 2013.
- [54] K. Jarrett, K. Kavukcuoglu, M. Ranzato, and Y. LeCun, "What is the best multi-stage architecture for object recognition?" in *Computer Vision, 2009 IEEE 12th International Conference on*. IEEE, 2009, pp. 2146–2153.
- [55] G. E. Hinton, N. Srivastava, A. Krizhevsky, I. Sutskever, and R. R. Salakhutdinov, "Improving neural networks by preventing co-adaptation of feature detectors," *arXiv preprint arXiv:1207.0580*, 2012.
- [56] I. Sutskever, J. Martens, G. Dahl, and G. Hinton, "On the importance of initialization and momentum in deep learning," in *Proceedings of the 30th International Conference on Machine Learning (ICML-13)*, 2013, pp. 1139–1147.
- [57] N. Neverova, C. Wolf, G. W. Taylor, and F. Nebout, "Moddrop: adaptive multi-modal gesture recognition," *arXiv preprint arXiv:1501.00102*, 2014.
- [58] N. C. Camgoz, A. A. Kindiroglu, and L. Akarun, "Gesture recognition using template based random forest classifiers," in *Computer Vision-ECCV 2014 Workshops*. Springer, 2014, pp. 579–594.
- [59] J. Y. Chang, "Nonparametric gesture labeling from multi-modal data," in *European Conference on Computer Vision and Pattern Recognition Workshops*, 2014.
- [60] G. D. Evangelidis, G. Singh, and R. Horaud, "Continuous gesture recognition from articulated poses," in *Computer Vision-ECCV 2014 Workshops*. Springer, 2014, pp. 595–607.
- [61] G. Chen, D. Clarke, M. Giuliani, A. Gaschler, D. Wu, D. Weikersdorfer, and A. Knoll, "Multi-modality gesture detection and recognition with un-supervision, randomization and discrimination," in *Computer Vision-ECCV 2014 Workshops*. Springer, 2014, pp. 608–622.
- [62] B. Liang and L. Zheng, "Multi-modal gesture recognition using skeletal joints and motion trail model," in *Computer Vision-ECCV 2014 Workshops*. Springer, 2014, pp. 623–638.
- [63] F. Bastien, P. Lamblin, R. Pascanu, J. Bergstra, I. J. Goodfellow, A. Bergeron, N. Bouchard, and Y. Bengio, "Theano: new features and speed improvements," in *Deep Learning and Unsupervised Feature Learning NIPS 2012 Workshop*, 2012.
- [64] A. Graves, M. Liwicki, S. Fernández, R. Bertolami, H. Bunke, and J. Schmidhuber, "A novel connectionist system for unconstrained handwriting recognition," *Pattern Analysis and Machine Intelligence, IEEE Transactions on*, vol. 31, no. 5, pp. 855–868, 2009.

Di Wu Biography text here.

Lionel Pigou Biography text here.

Pieter-Jan Kindermans Biography text here.

Nam Le Biography text here.

Ling Shao Biography text here.

Joni Dambre Biography text here.

Jean-Marc Odobez Biography text here.